Radiation Hardness of 4H-SiC Detectors for the CEPC Fast Luminosity monitor detector

D01

Jiaqi Zhou, Sen Zhao, Xin Shi, Weimin Song, Xiyuan Zhang
zhangxiyuan@ihep.ac.cn

Institute of High Energy Physics, Chinese Academy of Sciences

Motivation

Silicon carbide (SiC) is an ideal material for radiation monitoring in harsh environments due to its excellent properties, including low dark current, high breakdown voltage, high thermal conductivity, and strong radiation hardness. To systematically evaluate the performance of SiC-based detectors under realistic high-energy physics conditions, this study conducted irradiation experiments on two typical SiC detector structures:

- SiC Low-Gain Avalanche Detectors (LGADs) were irradiated with 80 MeV protons
- SiC PIN diodes were irradiated with 160 keV X-rays

By comparing the electrical characteristics , charge collection efficiency (CCE), and degradation mechanisms before and after irradiation, this work aims to validate the stability and durability of SiC detectors in high-radiation environments. The results will assess whether SiC-based detectors meet the stringent radiation hardness requirements for the Fast Luminosity Detector at the CEPC (Circular Electron-Positron Collider), providing critical experimental support for future detector selection in high-luminosity collider experiments.

Device Profile

SiC LGAD

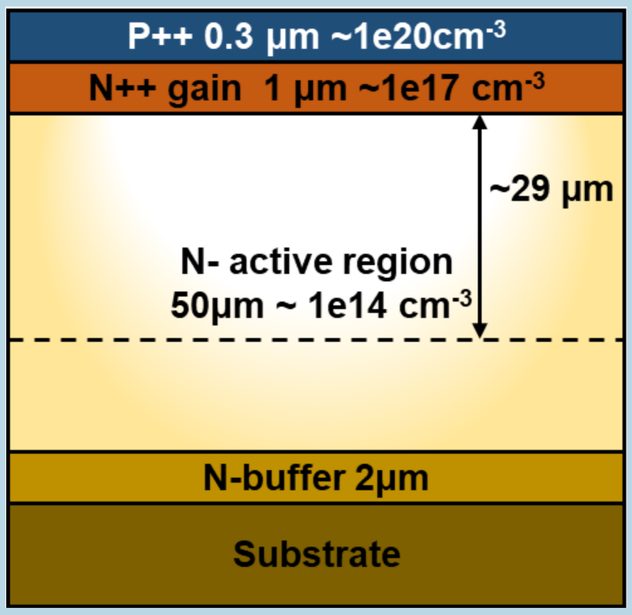

- **Irradiation conditions**: 80 MeV proton irradiation up to 7.0×10^{13} p/cm^2 in China Spallation Neutron Source (CSNS, Dongguan).

SiC PIN

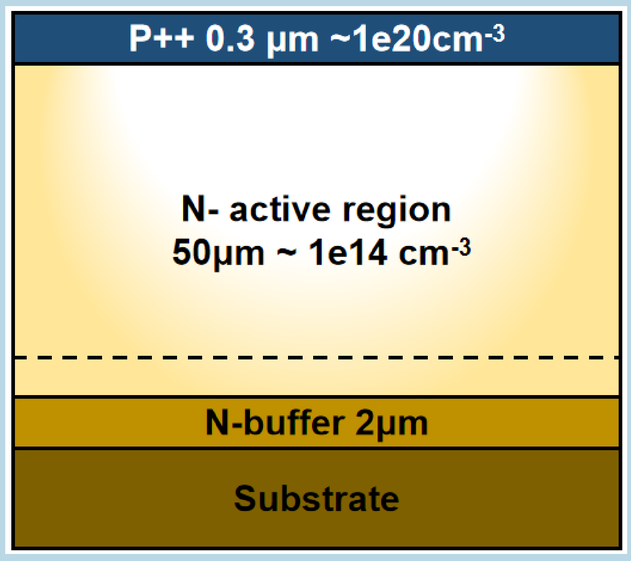

- **Irradiation conditions**: 160 keV X-rays up to 3.0×10^{21} p/cm^2 by Multi-Rad 160.

Test results for SiC LGAD and PIN

- **Leakage current and vs. bias voltage curve of SiC LGAD and PIN with radiation**:

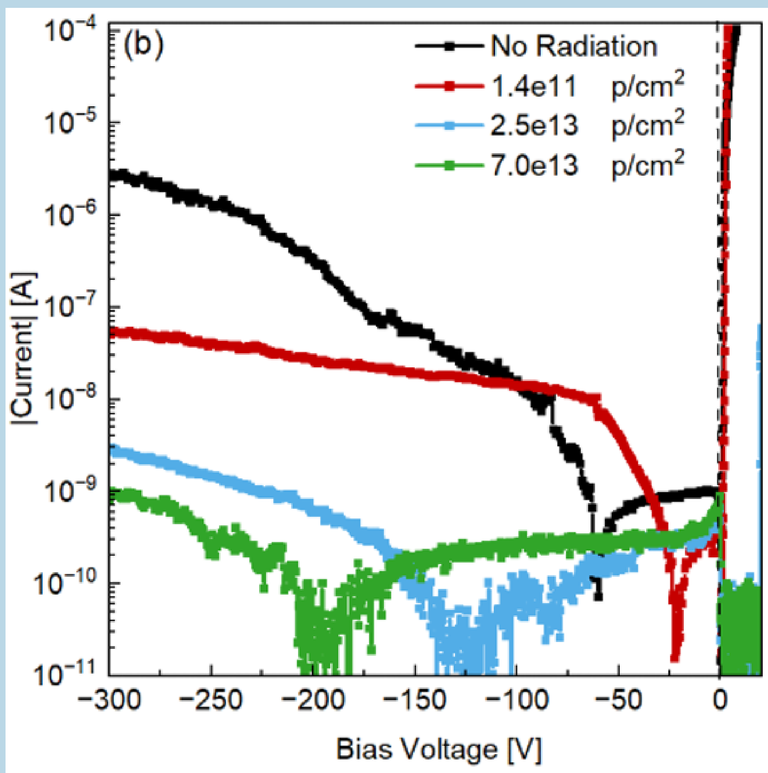

- IV curves of SiC LGAD under different proton irradiation fluences, showing a decrease in current with increasing fluence

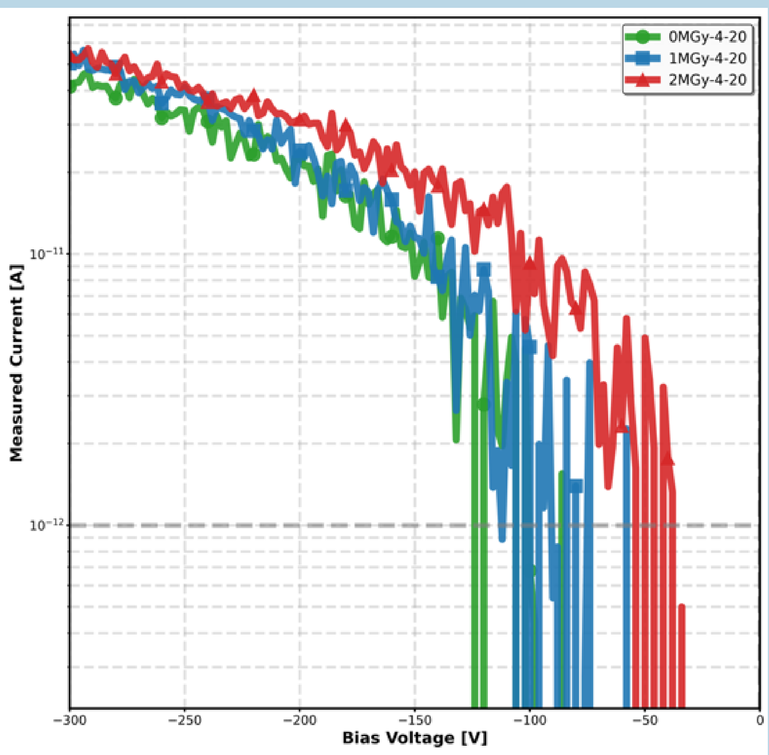

- IV curves of SiC PIN under different X-ray irradiation doses, showing almost no change in current even with increasing dose

- **The LGAD charge collect efficiency vs. proton radiation fluence**:

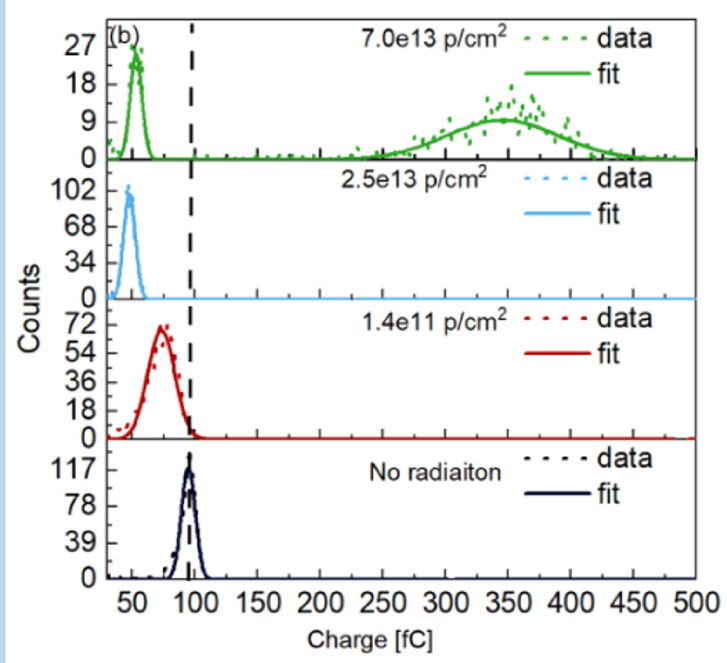

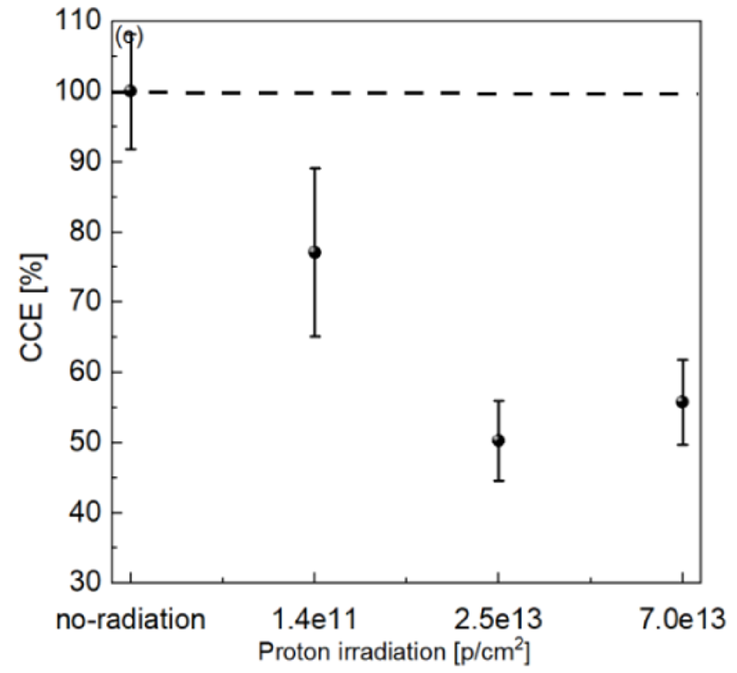

Under 7e13 proton fluence, the charge collection efficiency of SiC LGAD has decreased to 50%

- **The PIN charge collect efficiency vs. X-ray radiation dose**:

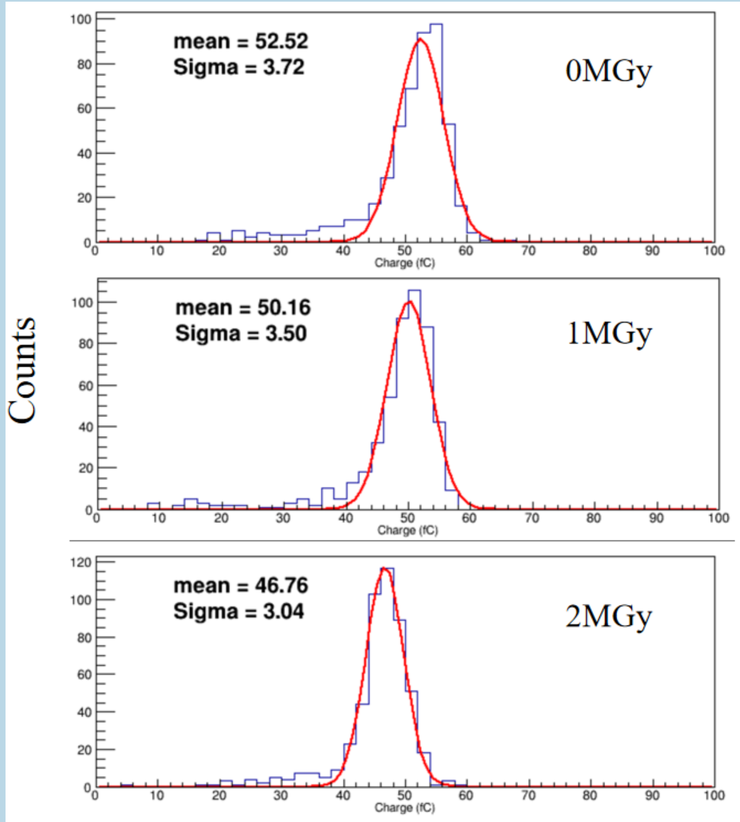

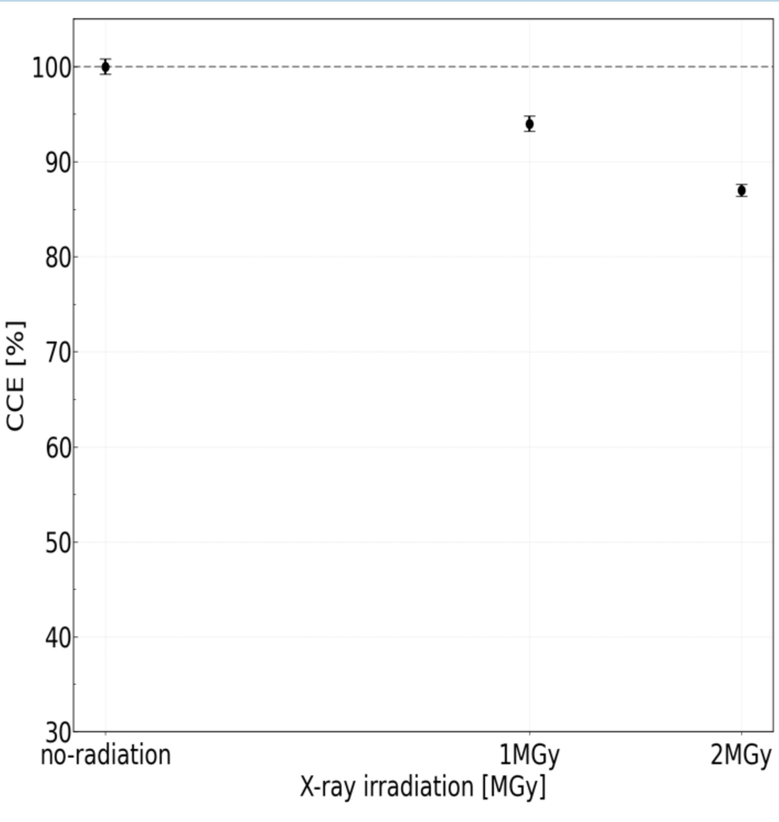

SiC PIN diodes maintain over 85% charge collection efficiency even after 2 MGy X-ray irradiation

References

Zhao, S. et al. The study of 4H-SiC LGAD after proton radiation. *arXiv:2507.12238* (2025).

D02

Electromagnetic Characteristics of an Aluminum-stabilized Stacked HTS Tape Cable No-Insulation Coil

Qingyuan Li[1,2], Yatian Pei[2], Menglin Wang[2], Yuanlong Ding[1,2] , Qingjin Xu[2], Wei Pi[1], and Feipeng Ning[2]
1) The State Key Laboratory of Alternate Electrical Power System with Renewable Energy Sources and the Key Laboratory of HV and EMC Beijing, North China Electric Power University, Beijing, 102206, China
2) Institute of High Energy Physics, Chinese Academy of Sciences, Beijing 100049, China

ABSTRACT

This paper presents an Aluminum-stabilized Stacked HTS Tape Cable (ASTC) solenoid coil for the Circular Electron Positron Collider (CEPC) detector. Its electromagnetic properties are systematically studied through experiments and simulations. Tests at current ramp rates of 0.2, 1, and 5A/s analyse voltage response and magnetic field delay. Results show the aluminum stabilizer significantly suppresses field delay, contrasting with no-insulation coils and enabling precise electromagnetic control. Finite element modeling examines how inter-turn contact resistance affects the time constant, refining the ASTC coil theoretical framework. This study provides experimental and theoretical insights into the electromagnetic response of ASTC solenoid coils, supporting the design and application of high-temperature superconducting magnets for the CEPC detector.

EXPERIMENTS

➢Test Coil and Experiment Conditions

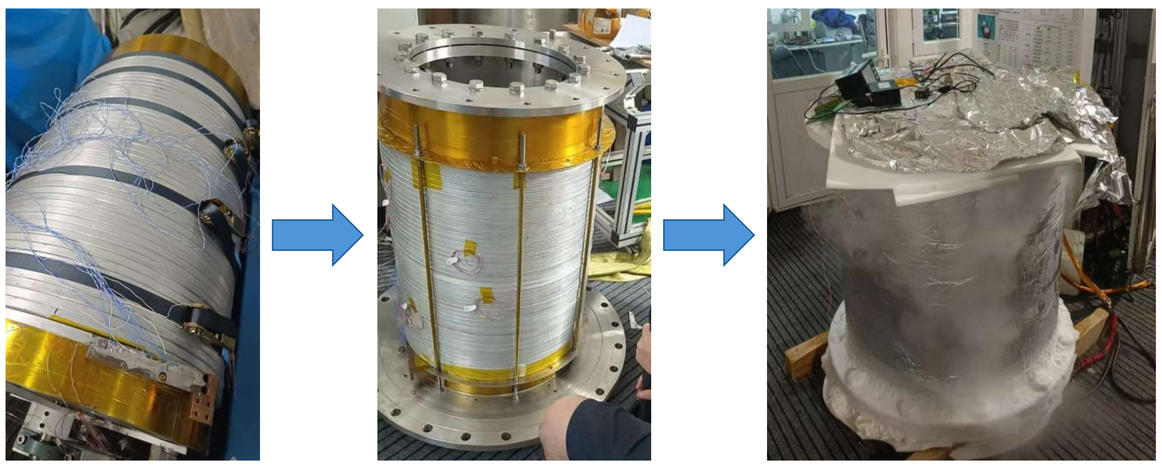

The coil was wound on a cylindrical mandrel with a radius of 300 mm, totaling 48 turns, and an axial preload was applied during winding using stainless steel strips. Performance testing was conducted with the coil immersed in liquid nitrogen, during which the current was ramped at rates of 0.2, 1, and 5 A/s up to 300 A.

Coil Parameters	Unit	Value
Cable Width	mm	15
Cable Thickness	mm	10
Number of REBCO Tapes	--	14
REBCO Tape Width	mm	4
REBCO Tape Thickness	mm	0.08
Critical current of ASTC (self-field@77 K)	A	450
Number of Turns	--	48
Inner Radius	mm	300

SIMULATION

➢3D Numerical model

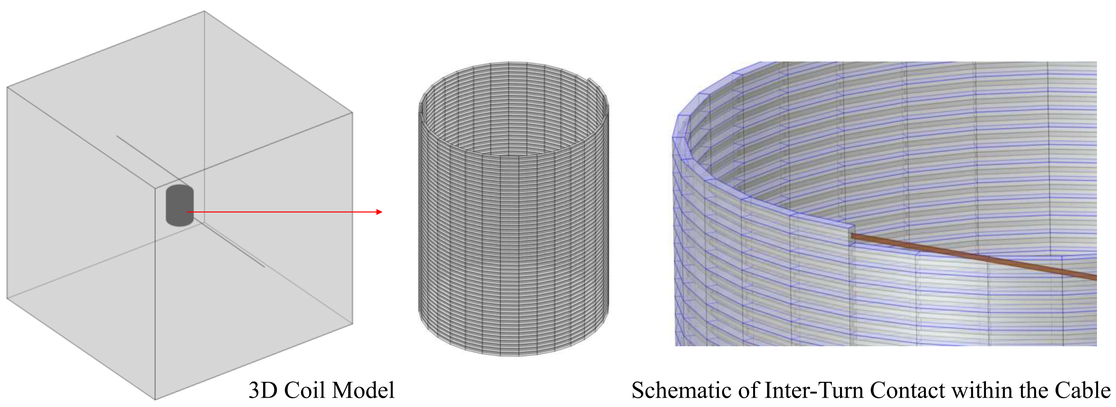

3D Coil Model

Schematic of Inter-Turn Contact within the Cable

Based on the experimentally measured surface resistivity between the superconducting tape and the adjacent turn in the cable (1.372×10^{-8} $\Omega\cdot m^2$), an equivalent inter-turn contact resistance was assigned in the model to accurately replicate the actual contact conditions during winding.

RESULTS AND DISCUSSION

The simulation results show good agreement with experimental data, confirming that the developed three-dimensional model accurately characterizes the electromagnetic properties of the ASTC coil. The findings demonstrate that the incorporation of an aluminum stabilizer effectively suppresses magnetic field delay, as evidenced by the coil's ability to rapidly reach the target magnetic field even under high current ramp rates.

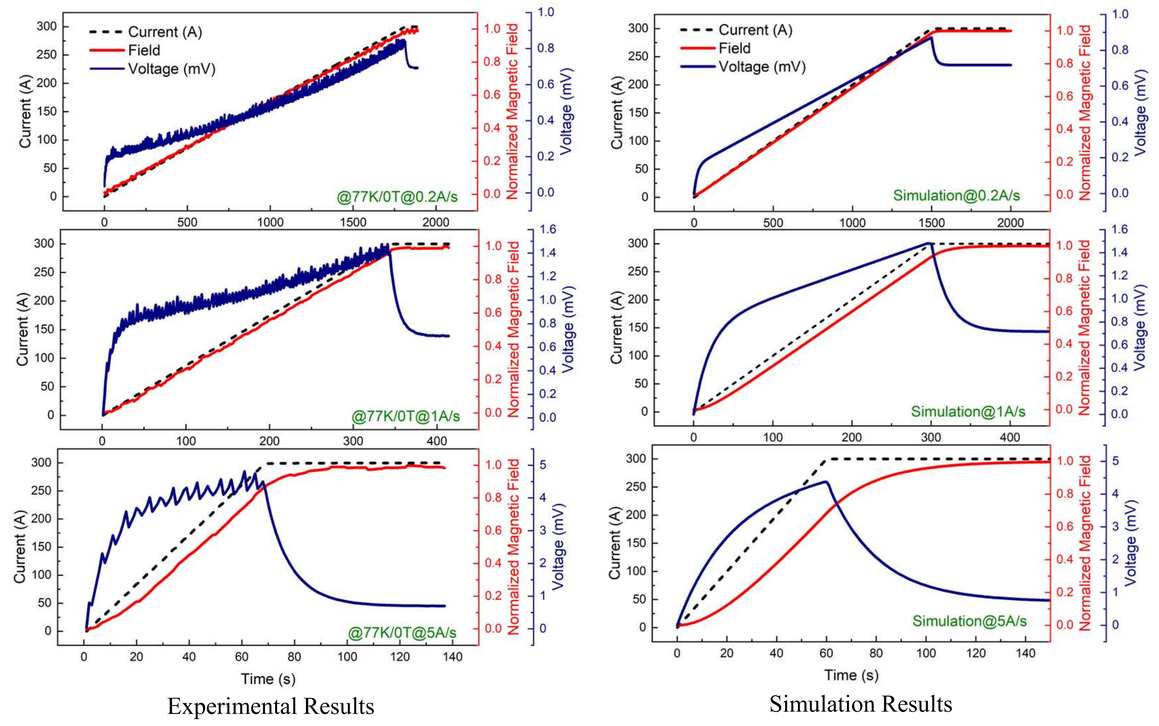

Experimental Results

Simulation Results

Higher current ramp rates enhance the inter-turn current sharing effect, leading to increased current flow through the aluminum stabilizer, thereby resulting in a corresponding rise in the coil's terminal voltage.

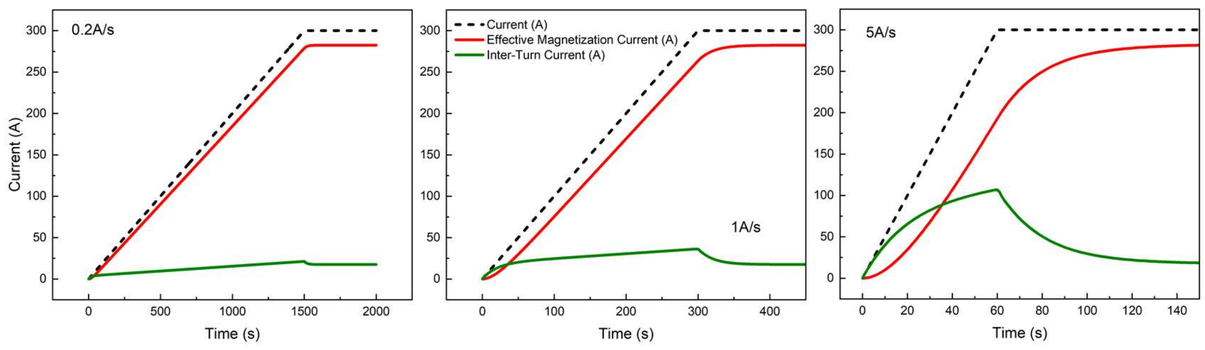

CONCLUSION

This study employs a combined experimental and simulation methodology to systematically examine how inter-turn contact resistance affects coil terminal voltage and magnetic field delay in ASTC coils. The findings advance the theoretical framework for understanding the electromagnetic properties of these coils. Moreover, this work establishes a solid experimental and theoretical foundation for interpreting the electromagnetic response of aluminum-stabilized high-temperature superconducting stacked cable solenoid coils, while also providing key insights for optimizing and implementing high-temperature superconducting magnet systems in the CEPC detector.

D03

Beam monitor online system design

BMOS readout design and DAQ plan

Sen Zhao, Xiyuan Zhang ,Xin Shi
The Institute of High Energy Physics of the Chinese Academy of Sciences
e-mail:shixin@ihep.ac.cn

Introduction

This work presents a beam monitor online system design for the 1.6 GeV proton beam at China Spallation Neutron Source (CSNS), based on silicon carbide (SiC) PIN sensors. Key aspects of the design include:

- **Halo detection strategy:** Detectors are placed outside the direct beam path (2×2 cm^2 core) to monitor particles at beam edge, minimizing damage of beam while reconstructing beam parameters.
- **Readout Electronics:** A charge-sensitive amplifier with CR-RC shaping circuit processes signals.

The system enables real-time monitoring of the instensity, position, and uniformity of the updgraded CSNS beam.

Design Objectives & Strategy

Key Objectives:

- **Real-time Monitoring:** Measure beam intensity, position, and uniformity with high precision
- **High Reliability:** Designed for 5,000+ hours/year continuous operation

Innovative Halo detection strategy:

- **Beam Center:** 2×2 cm^2 central zone
- **Peripheral Detection:** SiC detectors placed outside direct beam path
- **Key Advantage:** Monitors particles at beam edge to reconstruct beam parameters while avoiding direct damage of beam

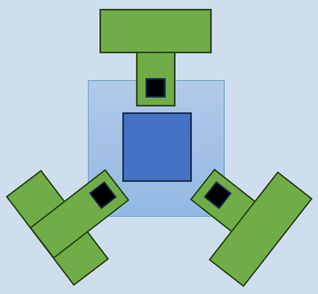

The layout of BMOS detector. It consists of 3 movable detector boards around the beam center

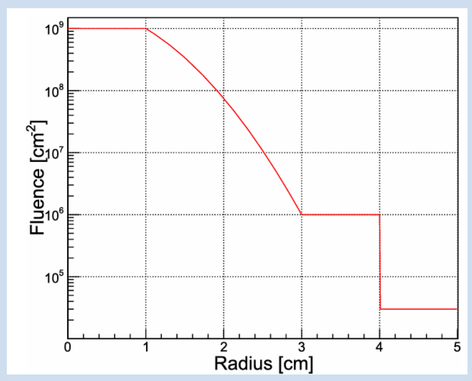

The relationship between radius and fluence

Sensor Features:

1. **Radiation Hardness:** 4H-SiC's wide bandgap and high atomic displacement threshold ensure stable operation in high-radiation environments
2. **Thermal Performance:** High thermal conductivity enables reliable room-temperature operation and effective heat dissipation

Beam Structure and Sensor Response

Macro Pulse Frequency: 25 Hz (24 Hz effective)

Macro Pulse Length: 1 ms, Interval: 39 ms

Micro-pulse in macro-pulse

Micro-pulse period: 410 ns, Micro-pulse Length : 80 ns

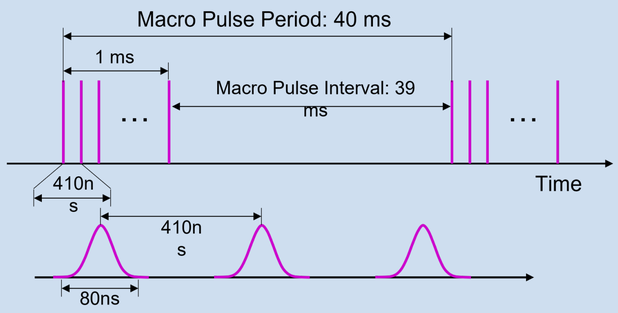

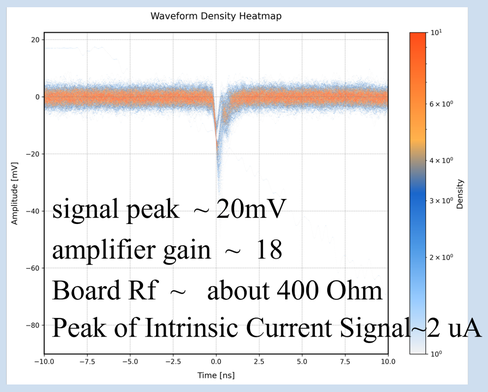

Total Read-out Design and Simulation

Readout design

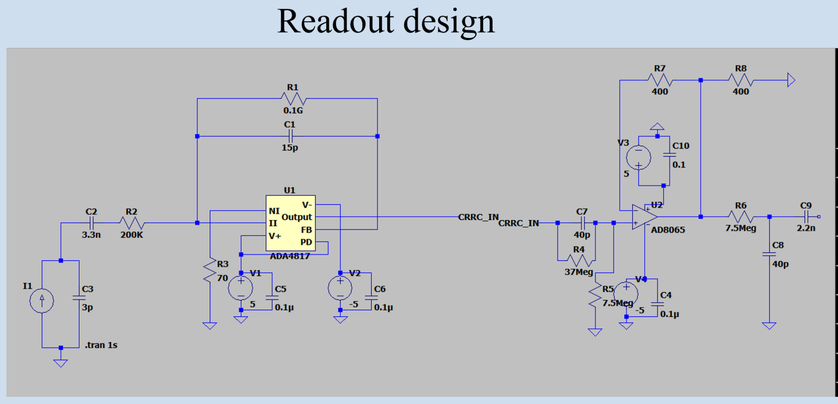

Signal simulation

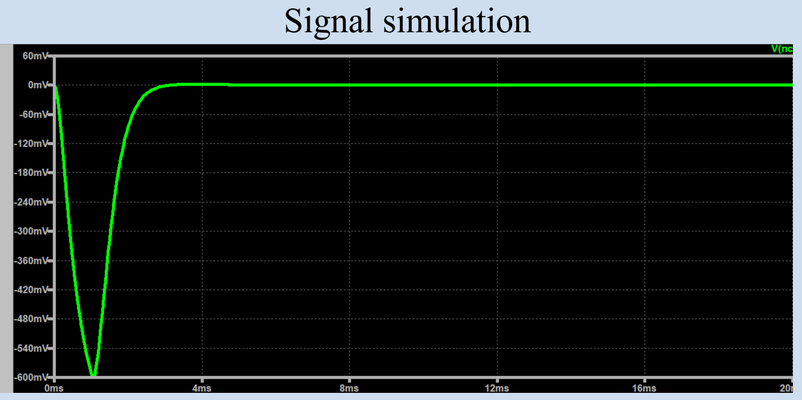

Charge-sensitive amplifier design with ADA4817 (Input resistance 500 GOhm, Open-Loop Gain 65 dB) (Integration capacitance 15 pF, Discharge time about 15 ms)

Measurement Result

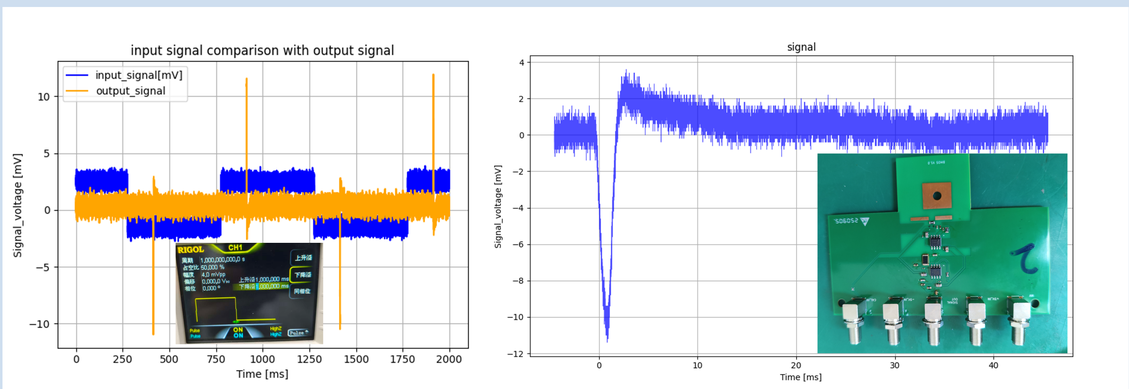

Signals generated by the signal generator are injected into the circuit board through the cal-in port, and the output of the circuit board is observed

Future Work Plan

- **Laser Testing:** Validate circuit board response using laser-simulated detector signals and optimize signal processing algorithms.
- **ADC/FPGA Development:** Implement ADC and FPGA-based real-time beam intensity calculation.
- **Vacuum Compatibility:** Modify board materials and layout for vacuum chamber integration and conduct stability testing.

References

1. He, Y. et al. High-precision CSNS beam monitor system conceptual design based on SiC. *Radiation Detection Technology and Methods* **8**, 1594-1603 (2024).
2. Yang, T. et al. Time Resolution of the 4H-SiC PIN Detector. *Front. Phys.* **10**, 718071 (2022).
3. Zhao, S. et al. Electrical Properties and Gain Performance of 4H-SiC LGAD (SICAR). *IEEE Transactions on Nuclear Science* **71**, 2417-2421 (2024).
4. Zhao, S. et al. The study of 4H-SiC LGAD after proton radiation. *arXiv:2507.12238* (2025).
5. Satapathy, Y. et al. Impact of Proton Irradiation on 4H-SiC Low Gain Avalanche Detectors (LGADs). *arXiv:2507.23062* (2025).

Poster ID: 276

The 2025 International Workshop on the High Energy Circular Electron Positron Collider (CEPC2025), Guangzhou, China, Nov 5-10, 2025

D04

Bhabha Event Acceptance of the LumiCal at CEPC

Jiading Gong[1] Weimin Song[1] Renjie Ma[2] Lei Zhang[3] Haoyu Shi[4] Suen Hou[5]

[1]Jilin University [2]Institute of Theoretical Physics, CAS

[3]Nanjing University [4]Institute of High Energy Physics, CAS

[5]Institute of Physics, Academia Sinica

Abstract

Small-angle Bhabha scattering (SABS) is the best calculated QED process as a reference channel for achieving ultra-high-precision luminosity measurements at electron-positron colliders. The event topology for detecting a pair of back-to-back scattered electron and positron has well defined detector acceptance, with precisely calculated cross-section. The "Circular Electron Positron Collider" (CEPC) is proposed to operate as a Higgs factory with $\sqrt{s} = 240$ GeV to deliver 1.2×10^6 Higgs boson events. It will also be running at Z-pole energy to produce 7×10^{11} Z boson events. The systematic uncertainties on luminosity must be contained to 10^{-4} to meet the stringent demands on Standard Model measurements. In this study, we have employed the BHLUMI event generator to evaluate detection of Bhabha scattering final state particles within the geometric acceptance of the LumiCal. The analysis focuses on characterizing the kinematics distributions of electrons and radiative photons for luminosity measurements.

Introduction

The design of the LumiCal is dedicated to ultra-precise forward-angle measurements with sub-millimeter spatial resolution, targeting the detection of Bhabha scattering events in the forward region. And currently, the only Monte Carlo tool with well-predicted behavior near the z-pole for SABS events is BHLUMI[1], developed based on the LEP experiment. It is solely based on QED principles and has a theoretical uncertainty of around 0.037% (refer to Table 2 in [2]). Therefore, BHLUMI is our preferred choice for predicting the physical outcomes obtained from the LumiCal.

The poster is structured as follows. In the section "SABS cross sections" , we compared the numerical results obtained for different LumiCal acceptance ranges and also examined the angular distribution of electrons. In the section "Radiative SABS", we analyzed the proportion of radiative SABS events and the behavior of radiated photons, aiming to control the errors inherent in QED theory itself through NLO measurements, thereby further enhancing the precision of CEPC luminosity measurements.

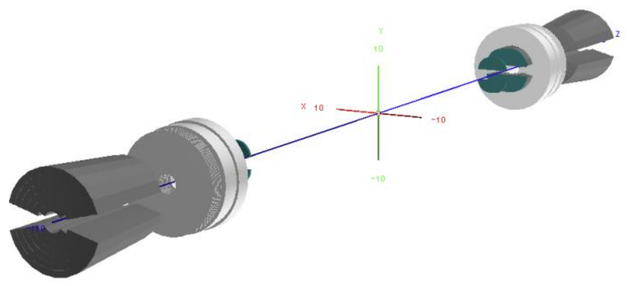

Figure 1. The geometry of LumiCal.

SABS cross sections

We generated 10^7 SABS events using BHLUMI, distributed across the ranges of 10–80 mrad and 10–120 mrad according to the CEPC operation plan.

Considering the 33 mrad cross-angle, Table 1, 2, and 3 present the corresponding cross section information at z = 1000 mm. Here, *r* represents the distance from the beam pipe for boosted particles, and *y* denotes the y-coordinate of particles when the z-axis coordinate is set to 1000 mm.

To ensure the accuracy of the cross section information, we also examined the distribution of electrons, as shown in Figure 2.

	CMS generated Th1, Th2(mrad)	$e^-.or.e^+$ to pipe centers (mm)	Single e^- in (mm)		Both $e^-.and.e^+$ in (mm)	
σ (nb)	10 to 80 1206.67	$10 < r, \lvert y\rvert < 80$ 1279.09	$20 < r$ 299.21	$.and.\ \lvert y\rvert > 20$ 141.52	$20 < r$ 286.90	$.and.\ \lvert y\rvert > 20$ 135.25
σ (nb)	10 to 80 1206.67	$10 < r, \lvert y\rvert < 80$ 1279.09	$25 < r$ 184.40	$.and.\ \lvert y\rvert > 25$ 84.64	$25 < r$ 176.19	$.and.\ \lvert y\rvert > 25$ 80.52
σ (nb)	10 to 120 1216.68	$10 < r, \lvert y\rvert < 120$ 1288.97	$25 < r$ 195.90	$.and.\ \lvert y\rvert > 25$ 94.14	$25 < r$ 187.75	$.and.\ \lvert y\rvert > 25$ 89.95

Table 1. The cross section at $\sqrt{s} = 91$ GeV.

	CMS generated Th1, Th2(mrad)	$e^-.or.e^+$ to pipe centers (mm)	Single e^- in (mm)		Both $e^-.and.e^+$ in (mm)	
σ (nb)	10 to 80 390.94	$10 < r, \lvert y\rvert < 80$ 416.14	$20 < r$ 97.21	$.and.\ \lvert y\rvert > 20$ 46.07	$20 < r$ 92.96	$.and.\ \lvert y\rvert > 20$ 43.90
σ (nb)	10 to 80 390.94	$10 < r, \lvert y\rvert < 80$ 416.14	$25 < r$ 59.93	$.and.\ \lvert y\rvert > 25$ 27.56	$25 < r$ 57.14	$.and.\ \lvert y\rvert > 25$ 26.14
σ (nb)	10 to 120 395.03	$10 < r, \lvert y\rvert < 120$ 420.23	$25 < r$ 63.83	$.and.\ \lvert y\rvert > 25$ 30.70	$25 < r$ 61.02	$.and.\ \lvert y\rvert > 25$ 29.23

Table 2. The cross section at $\sqrt{s} = 160$ GeV.

	CMS generated Th1, Th2(mrad)	$e^-.or.e^+$ to pipe centers (mm)	Single e^- in (mm)		Both $e^-.and.e^+$ in (mm)	
σ (nb)	10 to 80 174.33	$10 < r, \lvert y\rvert < 80$ 186.10	$20 < r$ 43.48	$.and.\ \lvert y\rvert > 20$ 20.58	$20 < r$ 41.49	$.and.\ \lvert y\rvert > 20$ 19.56
σ (nb)	10 to 80 174.33	$10 < r, \lvert y\rvert < 80$ 186.10	$25 < r$ 26.81	$.and.\ \lvert y\rvert > 25$ 12.31	$25 < r$ 25.50	$.and.\ \lvert y\rvert > 25$ 11.65
σ (nb)	10 to 120 175.99	$10 < r, \lvert y\rvert < 120$ 187.75	$25 < r$ 28.51	$.and.\ \lvert y\rvert > 25$ 13.72	$25 < r$ 27.21	$.and.\ \lvert y\rvert > 25$ 13.03

Table 3. The cross section at $\sqrt{s} = 240$ GeV.

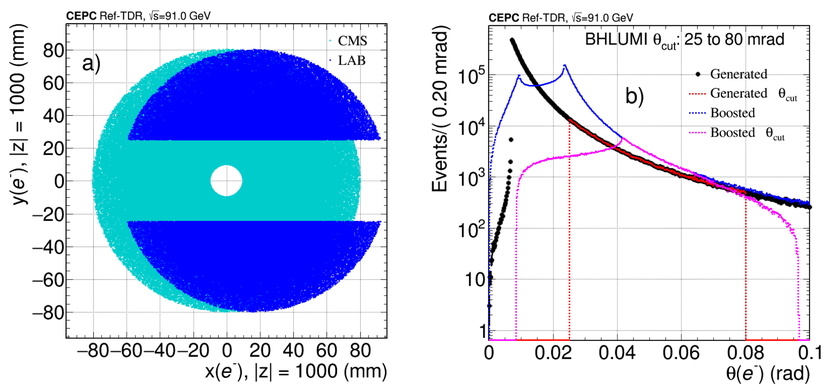

Figure 2. (a) The distribution of scattered electrons.
(b) The back-to-back angles between e^+ and e^- for both the generated and boosted events.

Radiative SABS

Next, we will focus on the Radiative SABS event.

When estimating cross section information, we also employed an alternative Monte Carlo event generator ReneSANCe[3]. The total cross section results from both methods differ only slightly, but they diverge in their description of radiative photons, as shown in Figure 3. As shown in Figure 3b, BHLUMI permits multi-photon generation, whereas ReneSANCe allows at most a single photon to be produced. This discrepancy also leads to inconsistencies in the behavior of high transverse momentum electrons between them (in Figure 3c).

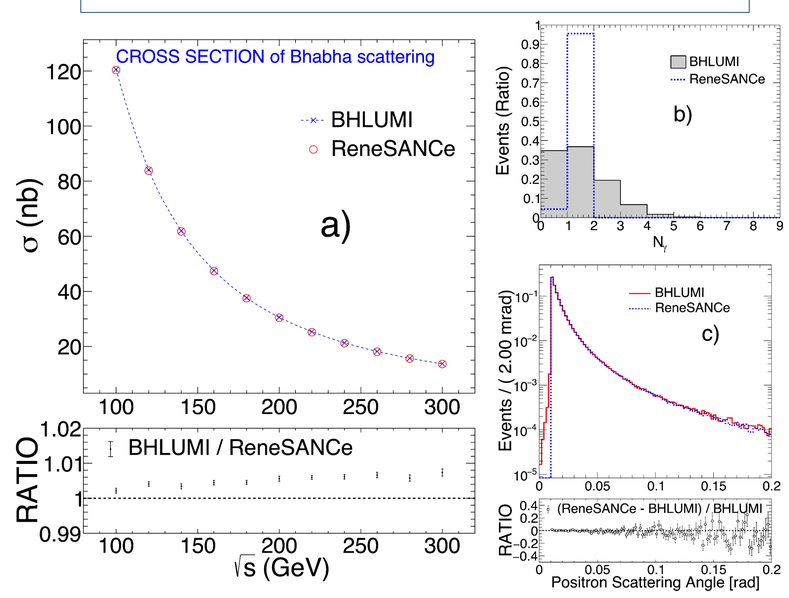

Figure 3. (a) Variation of the cross section with $\sqrt{s}$.
(b) The distribution of the radiative photon number .
(c) The angular distribution of positrons.

Given the practical constraints of the detector, we focus solely on the two photons with the highest energy. The corresponding angular distributions of photons relative to electrons are shown in Figure 4.

To better understand the radiative BhaBha process, we utilized BHLUMI to analyze the rate of multiphoton events at different working energy points for CEPC with the mentioned LumiCal structure.

At the same time, we require that the photon's energy $E_\gamma > 0.1$ GeV and the angle between the photon and the adjacent electron $\theta_{e^\pm\gamma} > 5$ mrad. The corresponding results are shown in Table 4 and Figure 5. Figure 5 illustrates the distribution of photons to ensure the accuracy of the cross section.

As can be seen, the cross section of the radiative SABS event is quite small within the luminosity monitoring range of the LumiCal. However, due to the extended operation of CEPC at z-pole, this presents a potential opportunity for NLO measurements.

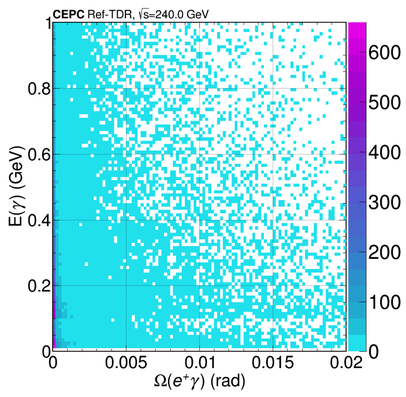

Figure 4. The angle between the photon and the adjacent positron $\theta_{e^+\gamma}$ *vs* the energy of photon E_γ.

	CMS (GeV)	Both $e^-.and.e^+$ in (mm)		ONE PHOTON	TWO PHOTON	NONE
σ (nb)	92.3	$20 < r$ 278.31	$.and.\ \lvert y\rvert > 20$ 131.11	7.97 (6.08%)	0.22 (0.17%)	122.91 (93.75%)
σ (nb)	160	$20 < r$ 92.96	$.and.\ \lvert y\rvert > 20$ 43.90	2.88 (6.56%)	0.09 (0.21%)	40.93 (93.23%)
σ (nb)	240	$20 < r$ 41.49	$.and.\ \lvert y\rvert > 20$ 19.56	1.35 (6.91%)	0.04 (0.20%)	18.17 (92.89%)

Table 4. The cross sections and event rates for single and double photon radiation at different $\sqrt{s}$.

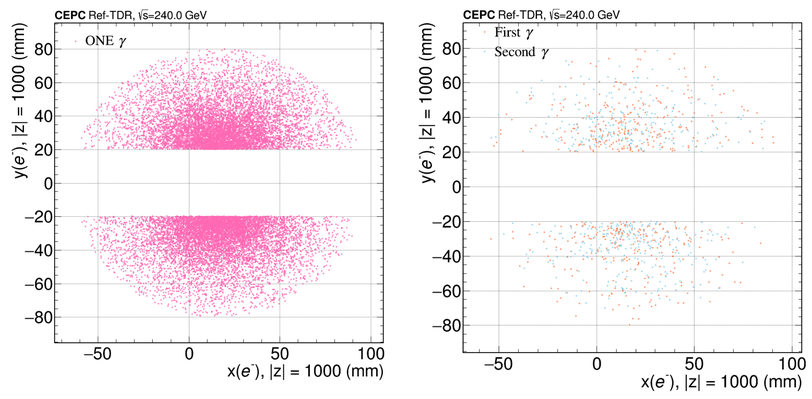

Figure 5. The distribution of photons for the single-photon events at z = 1000 mm (left) and the distribution of photons for the double-photon events at z = 1000 mm (right).

Conclusions

By integrating the design parameters of the LumiCal with the BHLUMI simulation framework, we accurately predict the cross-section information of Small-angle Bhabha Scattering events under the CEPC operation plan. Concurrently, addressing discrepancies in modeling radiative SABS processes with different generators, we preliminarily evaluate the measurability of radiative photon events. Furthermore, we propose an iterative optimization strategy for program parameters and detector calibration to enhance measurement precision. This work demonstrates that radiative SABS detection will set a new benchmark for precision luminosity monitoring at CEPC while advancing quantum electrodynamics (QED) validation through high-field electromagnetic interaction measurements.

Contact

Jiading Gong
Jilin University
Email: gongjd23@mails.jlu.edu.cn

References

[1] S. Jadach, W. Placzek, E. Richter-Was et al., Comput. Phys. Commun. **102**, 229 (1997)
[2] S. Jadach, W. Płaczek, M. Skrzypek et al., Eur. Phys. J. C **81**, 1047 (2021)
[3] R. Sadykov and V. Yermolchyk, Comput. Phys. Commun. **256**, 107445 (2020)

Simulation Studies of the Effect of SiPM Dark Noise on the Performance of a Highly Granular Crystal ECAL

D05

Jack Rolph, Yong Liu, Baohua Qi, Zhiyu Zhao
on behalf of the CEPC Working Group

中国科学院高能物理研究所
Institute of High Energy Physics
Chinese Academy of Sciences

Overview

Fluence At CEPC

- CEPC detector will endure unprecidented fluences during operation;

- $\Phi \approx 1\times10^{-10}$ cm^{-2} per year to beam pipe/at endcaps;

- Studies ongoing to reduce damage on instrumentation;

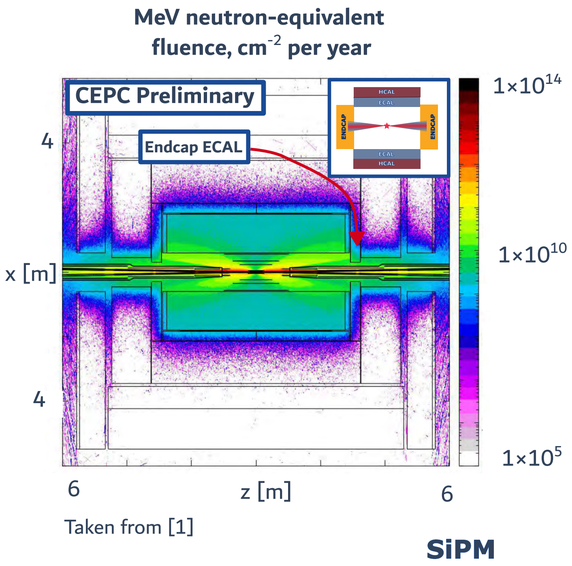

Taken from [1]

Highly Granular Crystal ECAL

- 40 cm scintillating crystal bars (BGO, BSO) provide;
  - granularity to separate individual particles;
  - excellent EM energy resolution (~1-2%/GeV)

- Light signal read out by **silicon photomultipliers;**

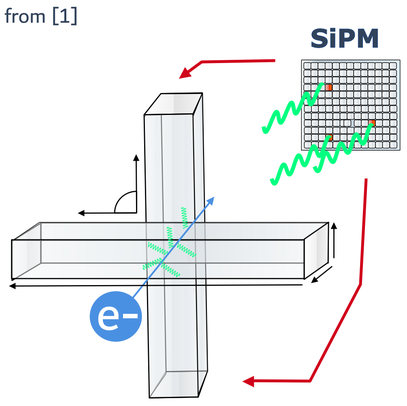

Silicon Photomultipliers (SiPM)

- Hadrons main source of damage for SiPMs (Non Ionising Energy Loss, NIEL);

- Crystal lattice displacement leads to **defects;**

- Defect-assisted trap-hole recombination → **dark noise;**

- **Dark noise degrades calorimeter performance;**

- **Additional signal from 'dark counts'**

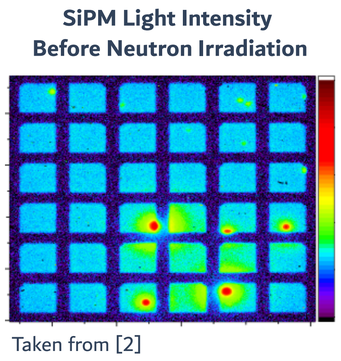

Taken from [2]

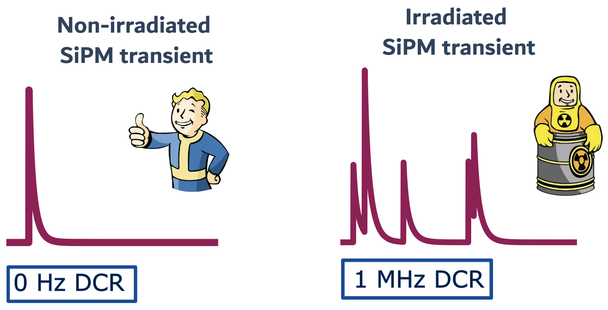

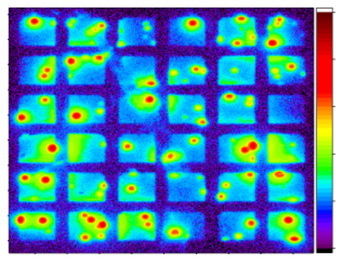

Taken from [2]

Summary of Study

Simulation

Particle showers
- Geant4 simulation;
- DD4HEP geometry description;
- 1 - 40 GeV electron showers;
- 1×10^{4} events per sample;
- Digitisation includes cross-talk and correlated noise;

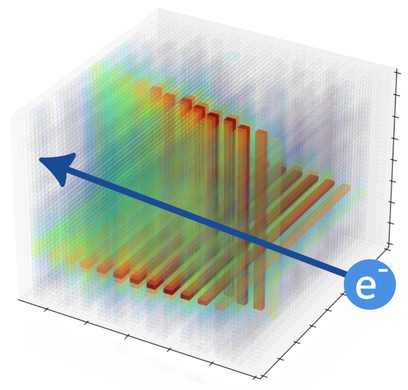

Dark Noise
- LightSimtastic SiPM simulation [2];
- DCR: 1 MHz - 1.58 GHz, log scale
- 1×10^{7} events per DCR sample;
- Resampled per event;

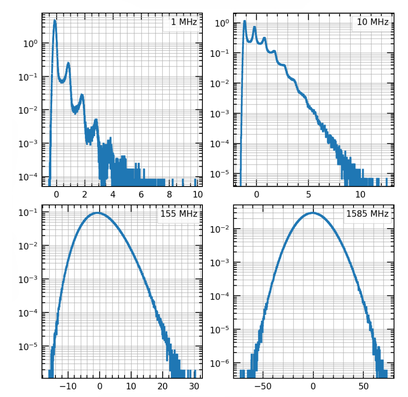

Analysis

- Dark noise combined with electron simulation using:
  - average crystal light yield, Φ= 200 p.e/MIP;
  - noise threshold, Q_{thresh} = 0.1 p.e;

$$Q_{\text{Signal+DCR}} = \begin{cases} \Phi_{\text{crystal}} \times E_{\text{sim}} + Q_{\text{DCR}} & \text{if } Q_{\text{Signal+DCR}} > Q_{\text{thresh}} \\ 0 & \text{otherwise} \end{cases}$$

- SiPM DCR related to fluence using study of Ref. [4];

- Resolution and linearity obtained using fits of Crystal Ball distribution to reconstructed energy;

Data taken from [4]

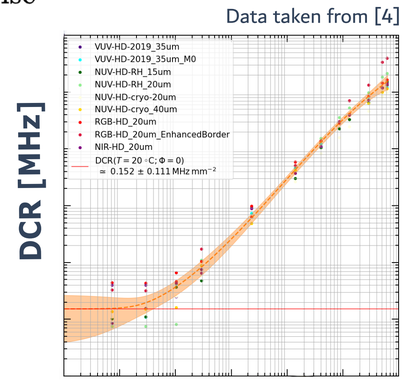

Key Question:

How does irradiation-induced dark noise degrade calorimeter resolution and linearity?

Key Results

Linearity of Response

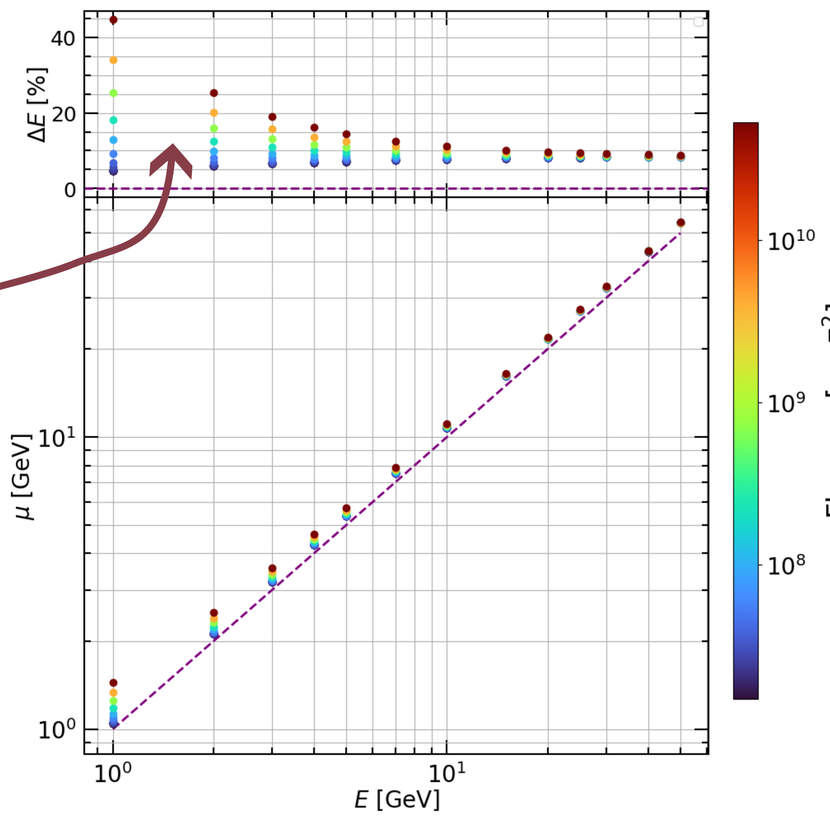

Linearity for <10 GeV showers degrades by up to 42% after around 1×10^{10} cm^{-2} fluence

Resolution

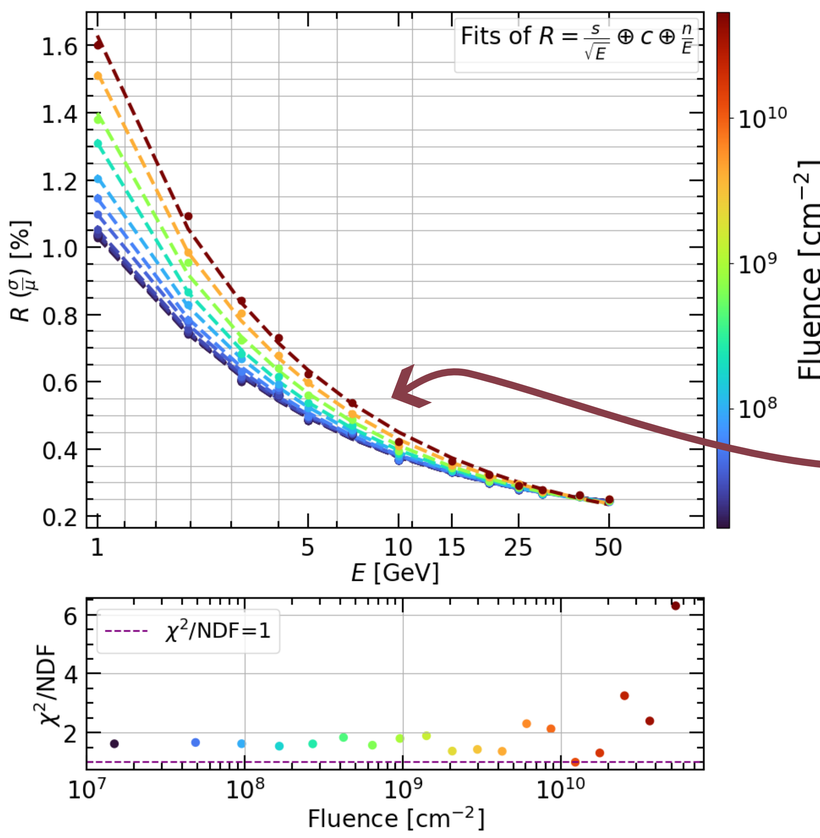

EM single-particle resolution degrades by ~0.5% after around 1×10^{10} cm^{-2} fluence

Take Home Message:

Radiation damage of SiPMs is a critical R&D issue for this calorimeter

[1] The CEPC Study Group, CEPC Technical Design Report -- Reference Detector, arXiv:2510.05260 [hep-ex] (2025), https://arxiv.org/abs/2510.05260.

[2] Engelmann, E., Popova, E., & Vinogradov, S. (2018). Spatially resolved dark count rate of SiPMs. The European Physical Journal C, 78(11), 971. https://doi.org/10.1140/epjc/s10052-018-6454-0

[3] UHH DetLab. (2025). LightSimtastic: A silicon photomultiplier simulation package [Computer software]. GitLab. https://gitlab.rrz.uni-hamburg.de/uhhdetlab/sipm/lightsimtastic

[4] Altamura, A. R., Acerbi, F., Di Ruzza, B., Verroi, E., Merzi, S., Mazzi, A., & Gola, A. (2023). Radiation damage on SiPMs for space applications. Nuclear Instruments and Methods in Physics Research Section A: Accelerators, Spectrometers, Detectors and Associated Equipment, 1045, 167488. https://doi.org/10.1016/j.nima.2022.167488

D06

Beam test results and simulation studies of high-density glass scintillator tiles

Dejing Du, Yong Liu, Baohua Qi, Sen Qian
Institute of High Energy Physics, Chinese Academy of Sciences
On behalf of the CEPC calorimeter team and Glass Scintillator Collaboration

Introduction

- **PFA-oriented calorimeter system: CEPC ref-TDR detector design**
  - Hadronic calorimeter (HCAL) with glass scintillator tiles
  - Expect better hadronic energy resolution than the plastic scintillator option
  - Requires glass scintillator to be dense, bright, cost efficient
- **R&D activities for glass scintillator HCAL**
  - HCAL design, simulation studies and hardware developments
  - Glass scintillator tiles: testing with cosmics/sources/beams
    - Key requirement: MIP response 60-100 p.e. in 10 mm thickness

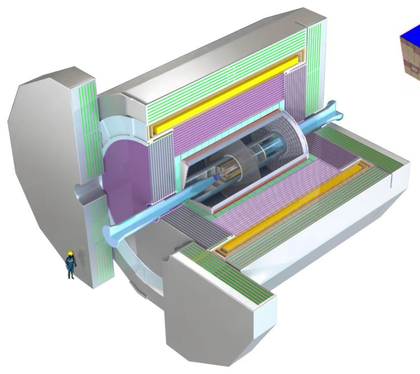

CEPC TDR reference detector

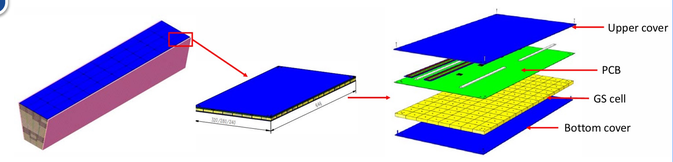

GS-HCAL sector structure

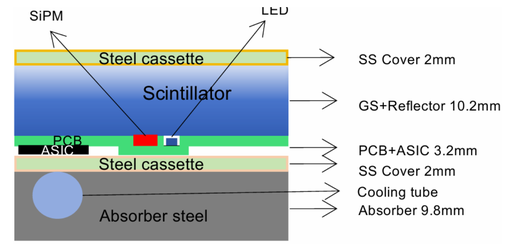

GS-HCAL single layer structure

Beam test results

- **Beam test for glass scintillator tiles**
  - 9 glass tiles with standard dimensions ($4\times4\times1\ \mathrm{cm}^3$)
  - Each glass tile coupled with one SiPM ($6\times6\ \mathrm{mm}^2$) at the center for readout
  - Successfully tested at DESY in Oct. 2023 with 5 GeV e^- beam

Glass tiles (standard size) before wrapping

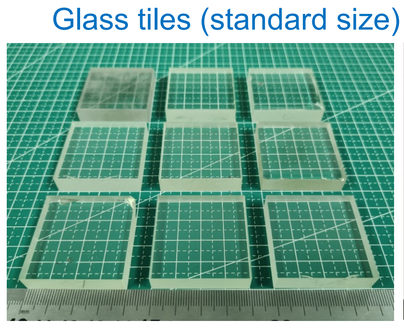

Glass tiles wrapped with Teflon and black tapes

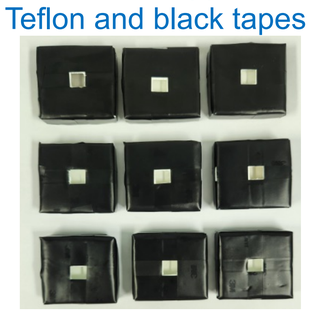

Beam test setup at DESY TB-22

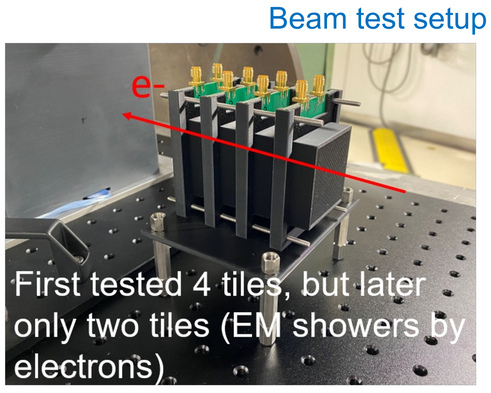

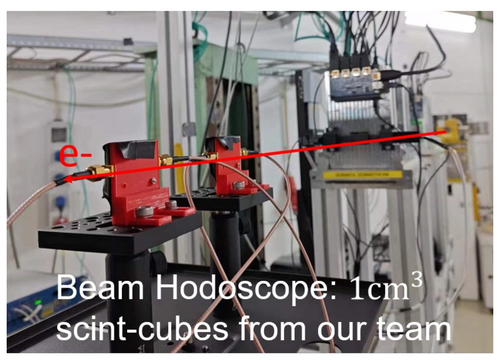

- **MIP response**
  - Observed clear (quasi-)MIP signals in all 9 glass tiles
    - The patterns in energy spectrum is largely due to tile response non-uniformity
  - Typical MIP response: 71–96 p.e./MIP, showed generally relatively good uniformity with the same batch

MIP spectrum of #4 sample

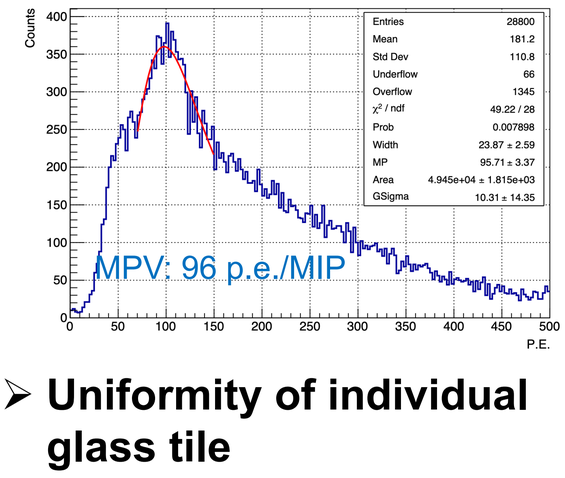

MIP response for 9 glass scintillator tiles

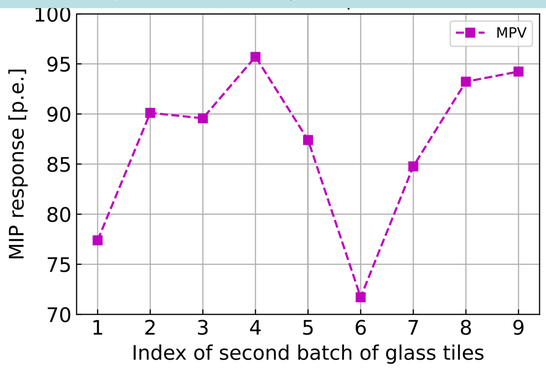

- **Uniformity of individual glass tile**
  - Vary beam incident position (1 cm step limited by trigger)
  - Non-uniformity ($\frac{max-min}{ave}$) is very large $\sim$200%
  - Improve it by optimizing tile design and glass material properties

Uniformity of #4 sample

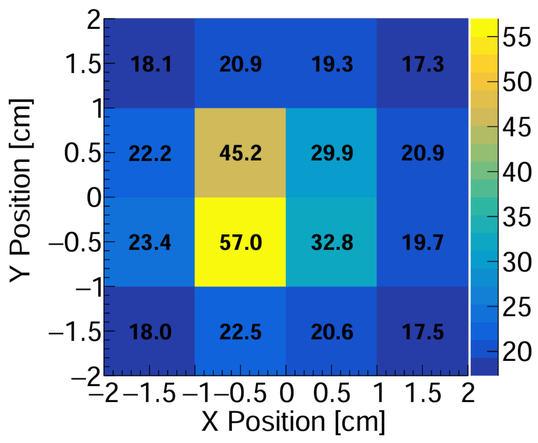

Optical simulation studies

- **Simulation Setup**
  - Including detailed geometry and optical processes
  - Properties of the glass tile extracted from measurements
  - Considering beam profile (2-D Gaussian distribution)

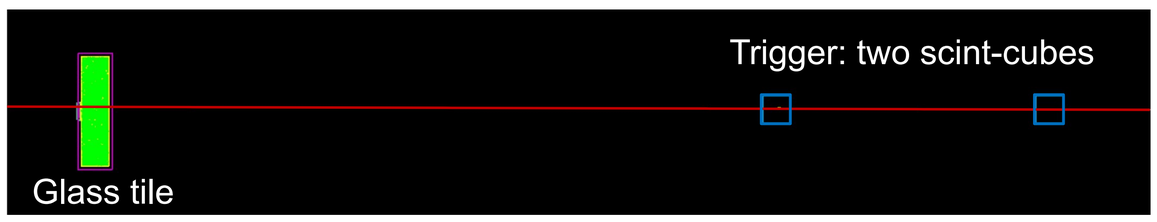

- **Simulation results**
  - For #4 glass tile, the discrepancy between test and simulation is smaller than 15%
  - The scattering effect cannot be ignored in glass scintillators, and the influence of scattering needs to be further considered in the simulation

MIP spectrum of simulation

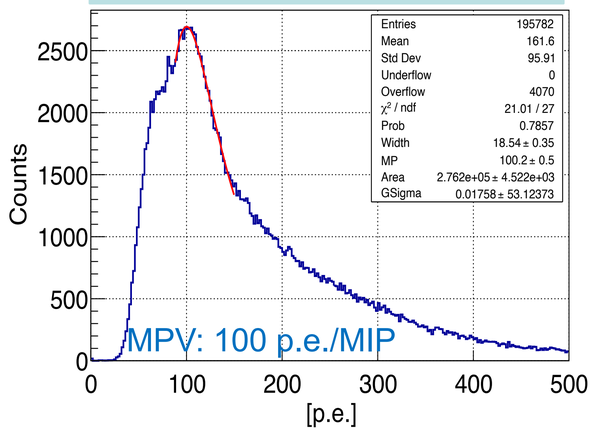

Tile uniformity of simulation

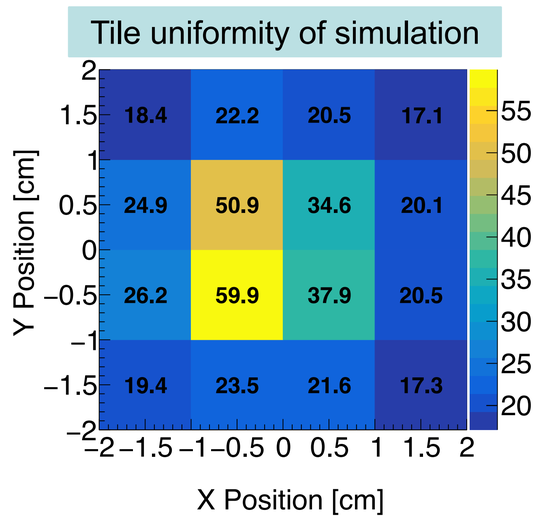

Difference between TB and MC

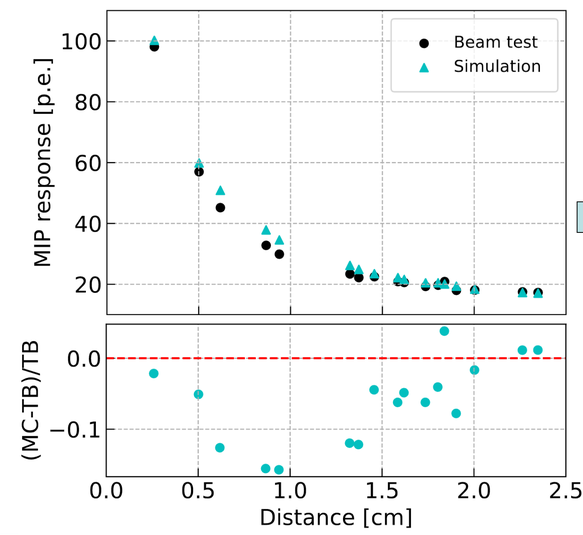

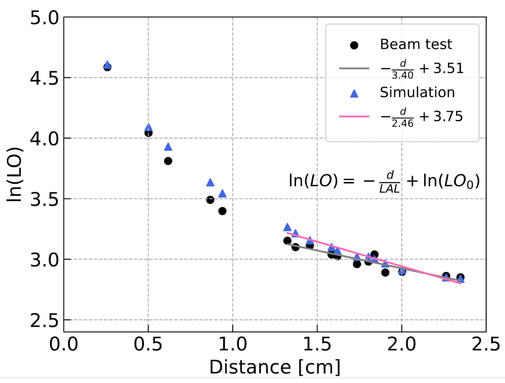

Summary

- Successful beam test with 9 glass tiles in standard dimensions, and results show the target of ~100 p.e./MIP in 10 mm thickness is very promising
- Ongoing efforts to improve TB/MC consistency through optimizing the optical simulation setup, and to improve tile uniformity by optimizing glass tile design

Acknowledgements: This work was received funding from the EURO-LABS. The authors would like to thank the technical support from beam test facilities of CERN and DESY and the DRD6 collaboration.

Beam test data analysis and simulation validation for the CEPC AHCAL prototype

D07

Dejing Du, Yong Liu, Baohua Qi
Institute of High Energy Physics, Chinese Academy of Sciences
On behalf of the CEPC calorimeter team

Introduction

➢ **CEPC Scintillator-Steel HCAL (AHCAL) prototype**
- 40 longitudinal layers, transverse sensitive size 72×72 cm^2
- Each layer: plastic scintillator tiles (40×40×3 mm^2) + steel absorber plate (2 cm) + SiPMs (HPK S14160-1315 and NDL-22-1515)
- 12960 readout channels, 360 SPIROC2E chips, ~5 ton in weight
- Developed during 2018-2022

➢ **Three beam test campaigns and data samples collection**
- Conducted at CERN (SPS-H8, SPS-H2, PS-T9) during 2022-2023
- Collected ~60M of beam test data samples
  - Muons: 160 GeV (H8), 100 GeV (H2), 10 GeV (T9)
  - Electrons/positrons: 20-120 GeV, 10-250 GeV, 0.5-5 GeV
  - Pions: 10-120 GeV, 10-350 GeV, 1-15 GeV

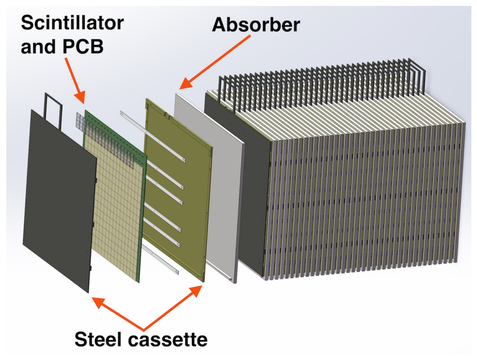

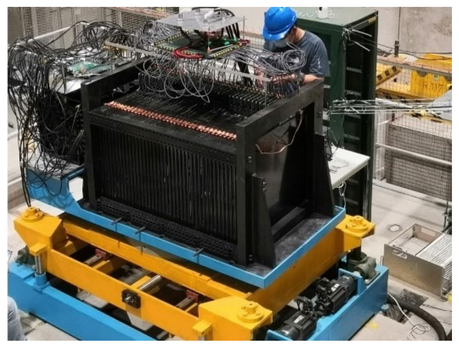

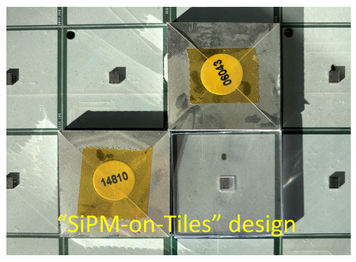

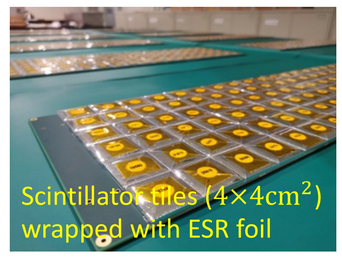

Simulation and Digitisation

➢ Geant4 simulation including detailed geometry AHCAL prototype
➢ **Digitisation:** energy depositions (Geant4) → digits in ADC (for each readout channel)

All parameters of digitisation extracted from test data

Geant4 hits: energy deposition → Scintillator-SiPM: detected photons → SiPM non-linearity → SiPM: p.e. convert to ADC → ASIC: ADC in High Gain or Low Gain

Pedestals (Electronics)

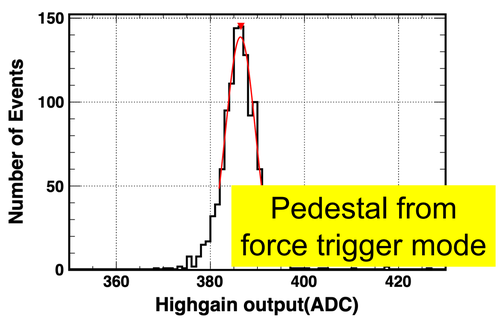

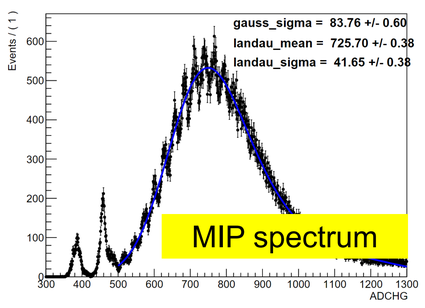

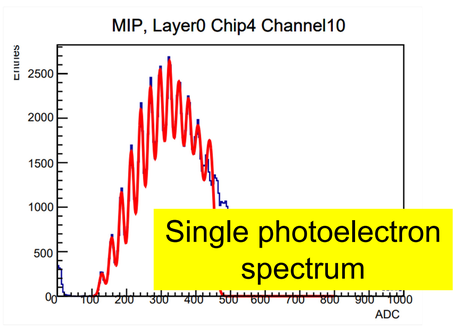

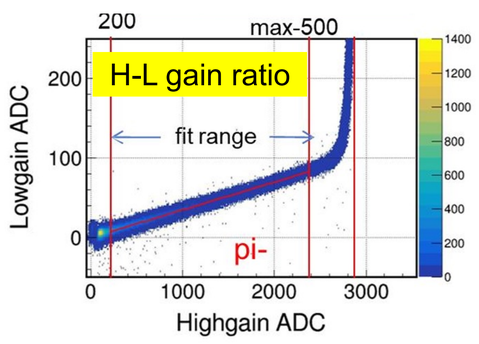

Simulation Validation Studies

➢ **Muon data:** good consistency
- MIP calibration: provide energy scale for each channel
- Crucial inputs for energy reconstruction of electrons and pions

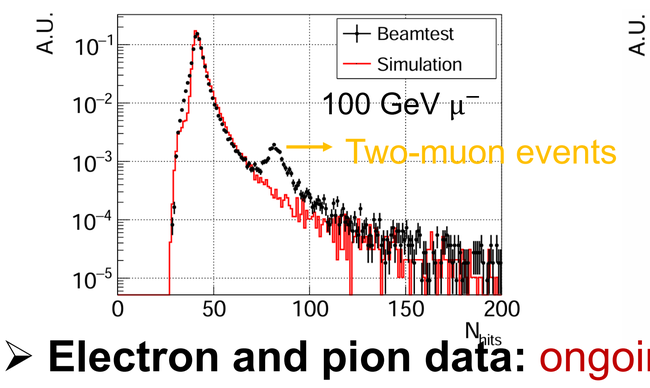

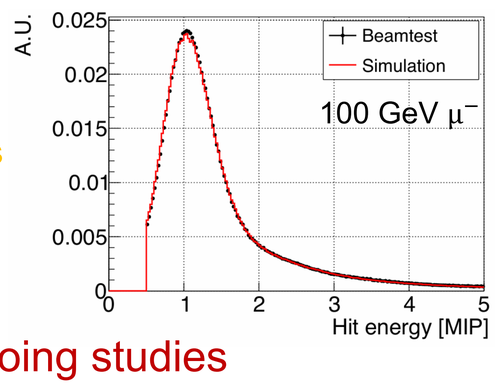

➢ **Electron and pion data:** ongoing studies
- Data/MC discrepancy: below 12% (e^-) and 14% (pi^-)
- Critical issue: non-linearity effects (saturations in SiPM and ASIC with large signals)
- Requires a better model for saturations effects in digitisation

Total Hit Number: Data/MC

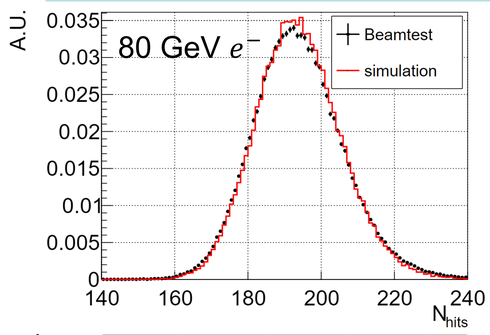

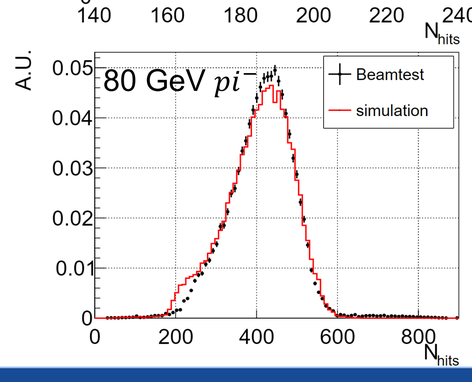

Energy Response: Data/MC

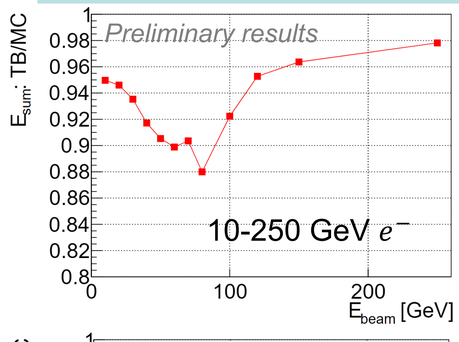

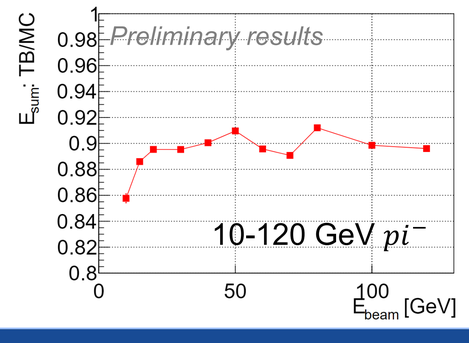

Performance

➢ AHCAL prototype using pion data sets after PID selections
- Energy linearity: within ±2%
- Energy resolution: $\frac{59.9\%}{\sqrt{E(GeV)}} \oplus 2.5\%$

Energy Linearity

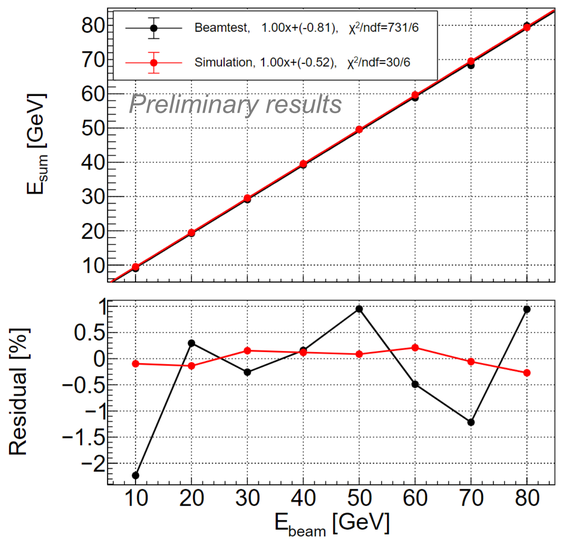

Energy Resolution

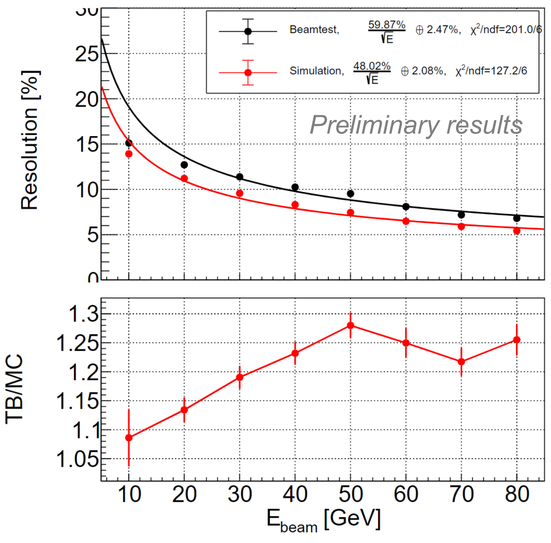

Summary

➢ Successful beam test campaigns at CERN PS/SPS during 2022-2023 collected decent statistics of data samples in the wide energy range
➢ Validation of the prototype simulation and digitisation using beam test data
➢ Ongoing efforts to improve data/MC consistency via better digitization models for non-linearity effects (SiPM and ASIC with large signals)

Design of the CEPC Gaseous Tracking Detector and Research on Particle Identification

Jianbo Zheng[1,2] Yue Chang[3] Huirong Qi[1] Xin She[1] Jinxian Zhang[1] Guang Zhao[1] Linghui Wu[1]
Qilin Wen[4] Haoyu Shi[1] Chengdong Fu[1] Gang Li[1] Manqi Ruan[1] Mingyi Dong[1] Jianchun Wang[1]

[1]Institute of High Energy Physics, CAS [2]University of Chinese Academy of Sciences [3]Central China Normal University [4]Tsinghua University

D08

Motivation & Background

1. Tracking Detector Challenge:

Table 1. CEPC Technical Design Report Physics Requirements for TPC

Parameter	Performance Requirement
Momentum resolution	$\sigma(1/p_T) < 10^{-4}\,(\mathrm{GeV}/c)^{-1}$
Magnetic field	> 3.0 Tesla
Spatial resolution	$\sigma_x < 100\,\mu$m
Track detection efficiency	$> 97\%$ (for $p_T > 1$ GeV)
Particle identification capability	$\pi/K > 3\sigma$ @ 20 GeV
dE/dx + dN/dx resolution	5%

2. **Research Objectives:** Optimize TPC structure, innovate PID algorithms, and validate prototype performance.

Design Scheme for the CEPC High-granularity Readout TPC

1. TPC Chamber Design

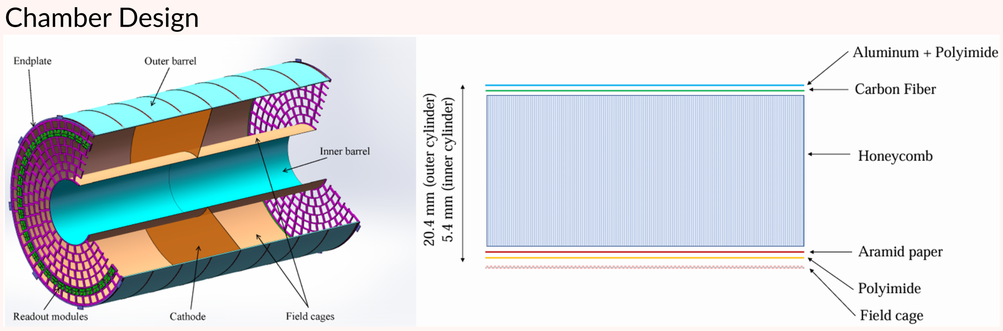

Figure 1. Schematic Diagram of CEPC-TPC Barrel Design and Structure

- Light Barrel: 0.69% X_0 for the outer cylinder and 0.45% X_0 for the inner cylinder wall.
- Outer cylinder: Lightweight composites (reduces weight, retains strength) + resistor-connected strips → electric field cage (uniform field).
- Inner cylinder: ∼ -62 kV central cathode (splits into 2 symmetric drift regions); endcaps/outer surfaces grounded.
- Endcaps: ≤147.5 kg, layered structure; space optimization ensures function in constrained dimensions.

2. Optimize the Readout Module

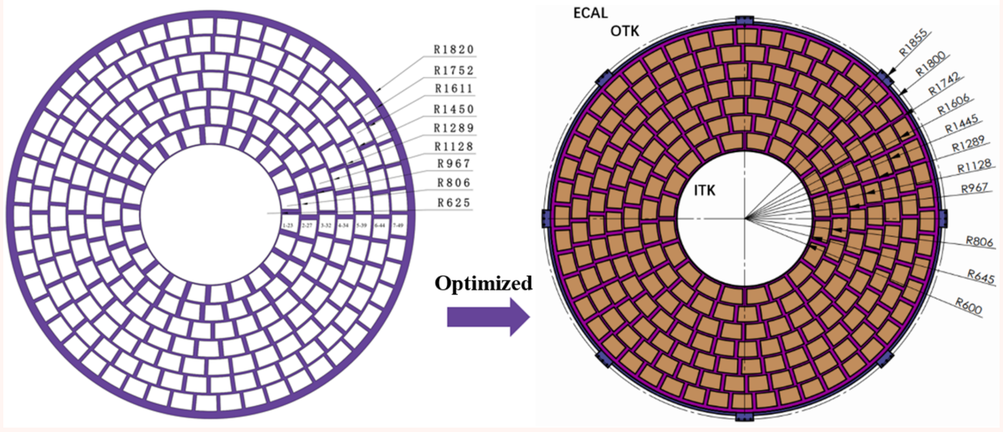

Figure 2. Schematic Diagram of the Readout Module Layout Before and After Optimization

For the readout endcap design, a modular annular layout is adopted—with repeated layout optimizations for annular regions of varying radii (R600 ∼ R1800)—to maximize the sensitive area. These optimizations boost the endcap's effective sensitive area from 92% to 96%, while 8 outer-edge mounting brackets further strengthen mechanical support and fixation.

3. Cooling System

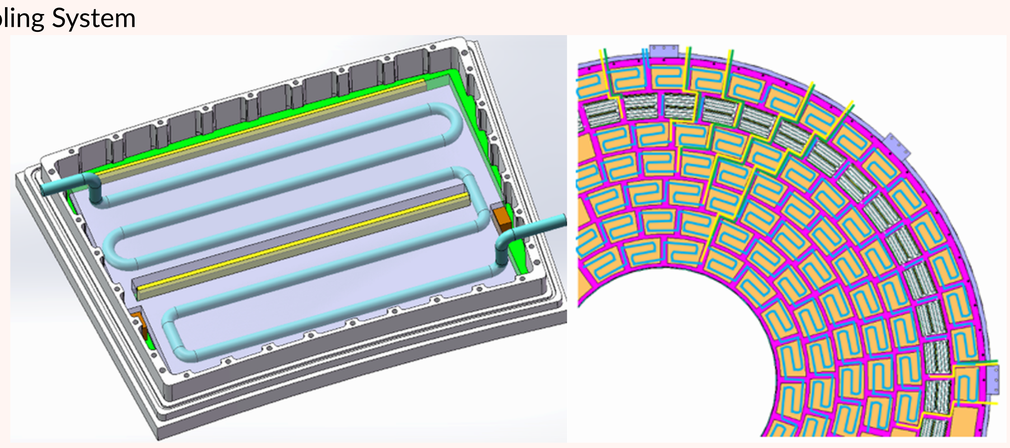

Figure 3. Cooling Scheme of Single Readout Module and Pipe Routing of Quarter Endplate

ASIC arrays cause about 10 kW/endplate power, needing thermal management; serpentine water tubes cool single modules (<28 °C ASIC temp), with 5 loops (12 modules/loop) per quarter-endplate, scaling to 21 parallel loops full endplate.

4. Readout Electronics System

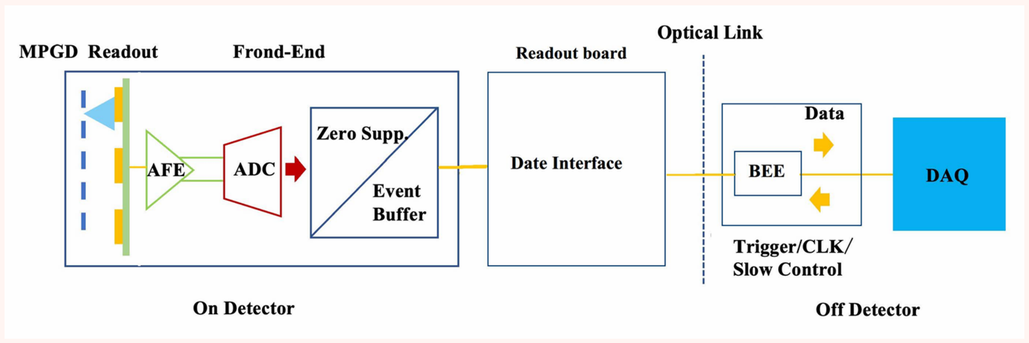

Figure 4. Architecture of the TPC Readout Electronics

TPC readout electronics has FEE (with AFE, ADC, DSP) on MPGD boards, sending signals to BEE/DAQ via high-speed optics.

Particle Identification Performance

Algorithm Optimization

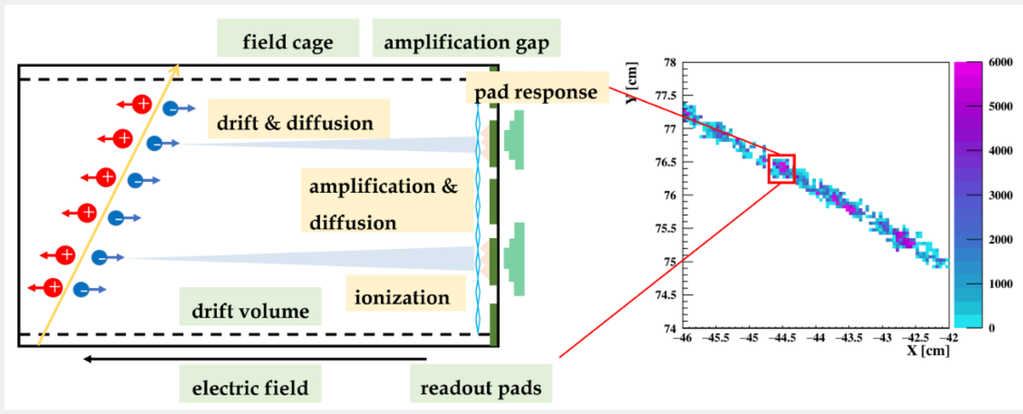

Figure 5. Schematic Diagram Illustrating the Operational Principle of the High-granularity Readout TPC

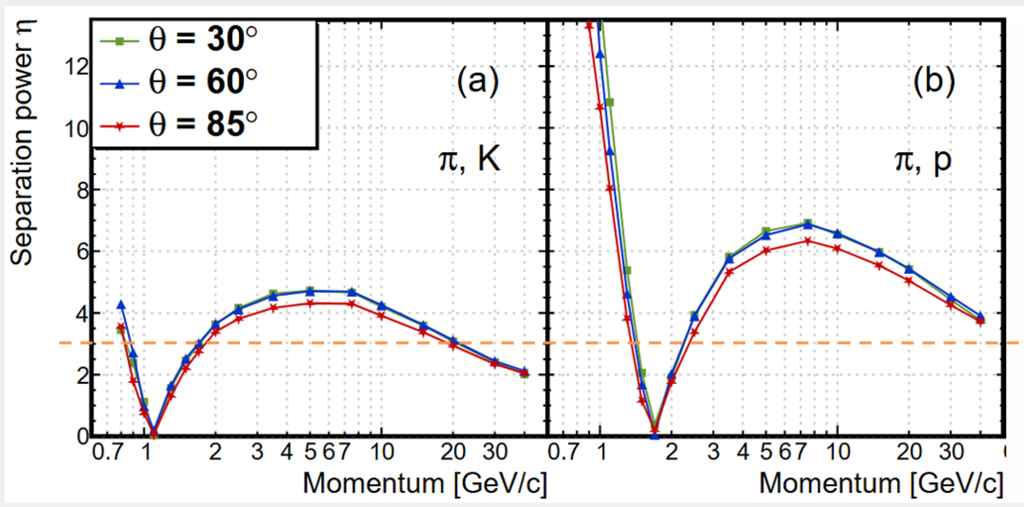

Figure 6. Separation Power of (a) π and K, (b) π and p

1. Optimization of Layer Merging

(a) Driven by dN/dx algorithm
- Fixed truncation ratio: 35% of ascending max value.
- Merged layers tested: 1–10.
- Optimal: 2 layers (balances spatial resolution & noise suppression, best discrimination).

(b) Driven by dE/dx algorithm
- Fixed truncation ratio: 40% of ascending max value.
- Merged layers tested: 1–10.
- Optimal: 1 layer (achieves best discrimination).

2. Optimization of Truncation Ratio

(c) Driven by dN/dx algorithm
- Fixed merged layers: 1.
- Truncation ratio tested: 0–40%.
- Optimal: 35% (suppresses noise, retains signals, best π/K discrimination).

(d) Driven by dE/dx algorithm
- Fixed merged layers: 1.
- Truncation ratio tested: 0–40%.
- Optimal: 40% (suppresses noise/secondary electrons, achieves best performance).

Optimization Results

Table 2. Systematic Optimization Parameters and Results Based on dN/dx and dE/dx Algorithms

Algorithm	Merged Layers	Truncation Ratio	π/K Particle Identification Capability
dN/dx	2	35% after ascending sort	3.48 σ
dE/dx	1	40% after ascending sort	3.34 σ

Optimization for 20 GeV π/K discrimination significantly improves PID performance vs. un-optimized data. Under θ=60°, 138 cm track length, both optimized algorithms meet CEPC's track detector requirements (20 GeV particle discrimination >3σ), with dN/dx algorithm having greater PID improvement potential.

Summary & Outlook

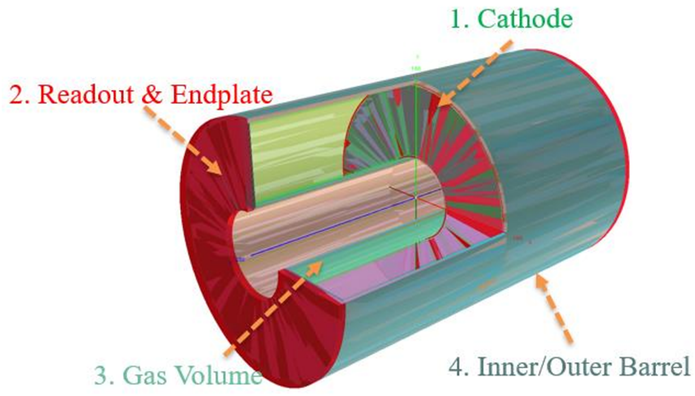

Figure 7. Simulation Framework of TPC Detector

1. **Study Coverage:** CEPC readout TPC (Design → Optimization → Testing).
2. **Key Innovations:**
   - Detector design: Performance optimization via multi-aspect tech innovations.
   - Particle identification: Proposed cluster counting (based on high-granularity pixel readout); compared dN/dx & dE/dx algorithm performance.
3. **Value & Future:** Provides key technical support for CEPC; future work: principle → engineering.

D09

The Construction of a Drift Chamber Prototype

The 2025 International Workshop on the High Energy Circular Electron Positron Collider 5th-10th Nov. 2025 Guangzhou

Jing DONG Mingyi DONG Xiaohui QIAN Fei HUANG Wenyu PAN

CAS-IHEP

Abstract

A drift-chamber-based design has been chosen and done as a possible alternative to the TPC, in order to contribute its PID performance in the CEPC reference detector's design[1].

Thanks to the nice collaboration with the ITA group[2], after the study of the simulation and the preliminary test, one short multilayer drift chamber prototype has been developed to study and optimize the resolution of $\mathrm{d}N/\mathrm{d}x$.

This work would like to report the construction of this short-multilayer drift chamber prototype including the key components and the construction standard during this work, as well as the experimentally measured results including wire-tension and leak current.

Induction

IHEP Drift Chamber:

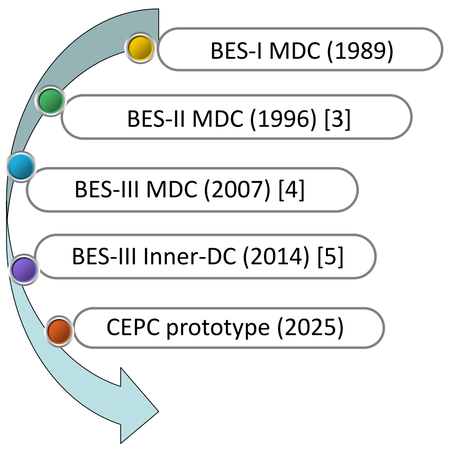

The design of the prototype

- Use of cluster counting for particle identification
- A cylinder + two end plates
- Length :~60cm
- 12 layers
- 10 cells/ layer
- 120 cells in total
- Cell size :18 mm x 18 mm
- Ratio of field wires to sense wires :3:1
- Sense wire :20 μm Au - plated tungsten
- Field wire :70 μm Aluminum

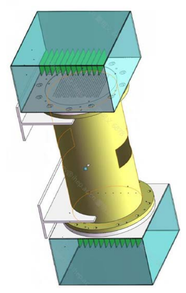

Construction

Prefers adopting the used skills of IHEP as much as possible:

1. Feed-through for the wire anchoring system;
2. Fully hand wiring, instead of the robot [6];
3. High standard of the precision mechanically(±25μm);
4. Wire feeding at almost closed cylindrical chamber , a big challenge to operate, keep clean and quiet (instead of endplates with few rods gaining open operation space)[7];
5. Trained a new hand wiring team;
6. Reestablish the connection to the industries;
7. … .

Major components

Feed through

Feed through:

It consists of three parts coaxially: inner-tube(1), outer-tube(2), and plastic tube(3).

1: Anchoring-Positioning various wires in the chamber.

2: Import/export-Cabling with high voltage and output signals.

3: Ensure insulation(LCP-A310).

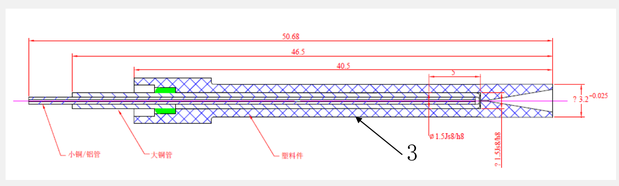

The design copies the BESIII's. Dimensions control within ±0.025 mm (diameter, coaxiality…）.

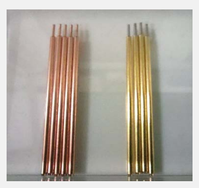

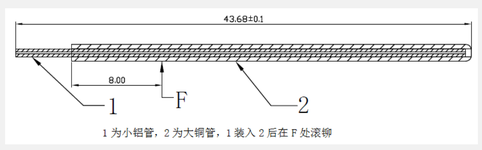

The connection between the inner/outer tube is achieved by using a special rolling riveting process（F）on the outer-tube, no adhesive.

The difference to the BESIII design: Add release forth(F) from 70g to 200g.(Resist~5.8m wire)

- The connection to the domestic industries has been reestablished.
- New feed throughs have been tested in a module.
- Tests of the conductivity(1&2), insulation(2&3), dimensions, gas tight(2&3), release force(1&2), have shown the new process could satisfy the requirements.
- The crimping shows no wire broken or tension lost happened for more than six months.
- Total 5k feed throughs have been produced and delivered.

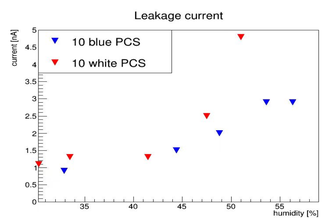

Leak current<1 nA
A good insulated performance.

Crimping

- The wire is fixed inside the feed-through by a special crimping.
- After inner-tube of feed through is crimped, the crimp parameter should be a relatively fixed value which had been optimized as the best performance of the wires.
- The localizational tool (Cleo design) has been adjusted to fulfil the task.

The crimp parameter:
Thickness:0.46mm
Width:0.85mm
Length:1.8mm

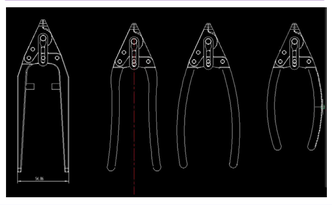

Wire

Wires:

- Luma Tungsten AU-plated:20μm
- CFW Al5056: 70 μm
- CFW Al5056 NI AU-plated: 80μm

$$T(c) = \lambda L^2/(8S_{ag})$$

λ : Linear density
S_{ag} : Wire deflection
L :Wire length

Parameters as 5.8 meter（Preliminary）

S/F	Diameter（μm）	Linear Density (10^{-5}g/cm）	Length（m）	Sag（μm）	Wire tension (Sag=450μm）（g）	Wire Break（g）
F	110	32.67	5.8	450	305	350-355
F	80	17.88	5.8	450	167	190-195
F	70	10.33	5.8	450	96	104-106
S	20	6	5.8	450	56	67-70

Connector

- The connector is used with the feed through for cabling.
- Total 3k connectors have been produced and delivered.

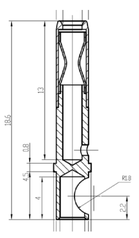

Wire Feeder

The wire has been fed vertically with two six-dimension tools in a no-visualized condition.

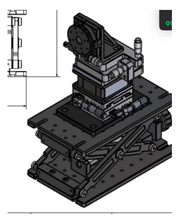

Status

1. Finished wiring, accuracy on the position of the wires < 50 μm (Mechanically).
2. Sense wire tension :11.94±0.31g, Sag :25μ m
   Field wire tension :19.91±0.04g, Sag :25μ m
   Wire tension distribution shows a good uniformity of the wire tension.

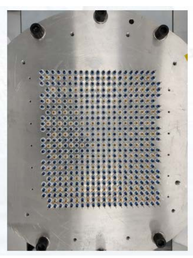

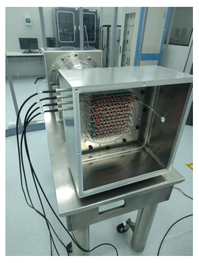

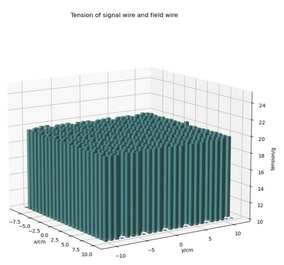

3. Finished the prototype construction, gas tightening, cabling and HV training.
4. Measurements with cosmic-ray (at IHEP)
   -> channel equalization, module calibration and system performances…

See Wenyu PAN's talk

Wire tension

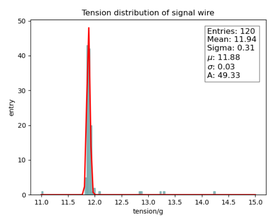

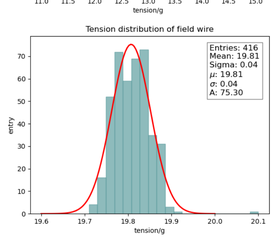

Acknowledge

The authors would like to thank BESIII-MDC and inner-DC group for the helpful record on the technology. This work was supported by the National Natural Science Foundation of China (12475192) and the State Key Laboratory of Particle Detection and Electronics (SKLPDE-ZZ-202408).

Reference

[1] CEPC Reference Detector Technical Design Report

[2] CEPC_workshop_Procacci,Barcelona,16Jun.2025

[3] Master thesis of Jundong Huang

[4] BESIII Preliminary Design Report, 2004

[5] Zhonghua QIN, https://arxiv.org/pdf/1312.0221

[6] R.Assiro et al., Nucl. Phys.B(Pric.Suppl.),248-250 (2014) 124-126

[7] Zhonghua QIN et al., HEP & NP,31(2007)4

Fast Simulation of the CEPC Long-Bar Crystal Electromagnetic Calorimeter

Li Zhihao [1 2] Lin Tao [1 2] Li Weidong [1 2]

[1]Institute of High Energy Physics [2]University of Chinese Academy of Sciences

D10

Introduction

- **CEPC** pursues staged Higgs, Z, and top programs that demand extremely high electroweak precision and sensitivity to rare decays, driving unprecedented detector-model fidelity and simulated data volumes.[1]
- **ECAL** The long-bar crystal ECAL forms an interleaved three-dimensional mesh that delivers about 3% energy resolution with fine imaging. [1]
- **Simulation Framework** The simulation workflow includes physics event generation, Geant4 based detector simulation, and digitization. The framework adopts a Gaudi-based modular architecture that integrates Geant4 . It is designed with pluggability, allowing the fast-simulation (FastSim) module to be selectively activated when specific particles enter the ECAL.

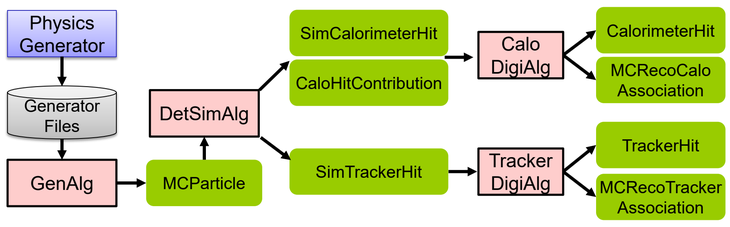

Figure 1. Overview of the CEPC Full Simulation Workflow.

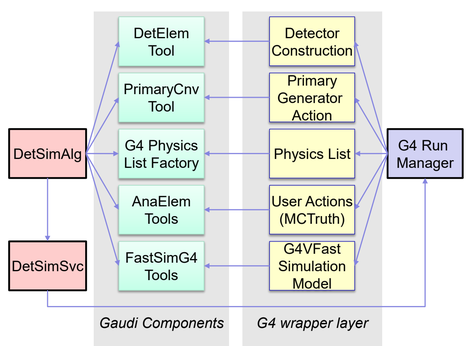

Figure 2. Architecture of the CEPC Simulation Framework and Fast Simulation Integration Points.

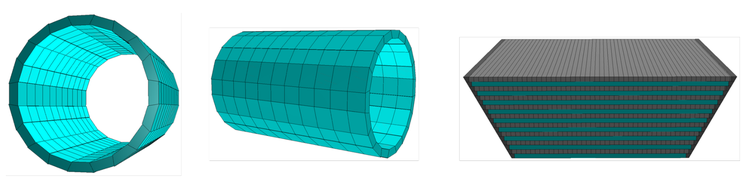

Figure 3. Geometry of the CEPC long-bar crystal ECAL Barrel.

Computing Bottlenecks

- **Classical Computing Resource Bottleneck:** The CEPC full-simulation program is expected to produce about $\mathbf{10^{11}}$ events per year, yielding 284 PB of full-simulation data and consuming roughly $\mathbf{1570}$ kHS23-yr of CPU computing time annually.[1]
- **Geant4 and ECAL Simulation Bottlenecks** For $e^+e^- \to q\bar{q}$ at 240 GeV the Geant4 step dominates 46.4% of the wall time; ECAL barrel and endcaps alone consume 34.4% and 13.8% of the total simulation budget, respectively.
- **Digitization and Optical Photon Challenge** Digitization currently relies on semi-empirical parameterizations that already take 25% of the workflow; introducing optical photon tracking based on Geant4 would be prohibitive, so Opticks-based ground truth is needed for training alternative models.[2, 4]

Run stage	MC events	CPU time (kHS23-yr)	MC data (PB)
Higgs	2.0×10^9	105	4.00
Low Z	1.4×10^{11}	1465	280.00

Table 1. Projected CEPC **annual** simulation throughput and storage requirements by run stage.

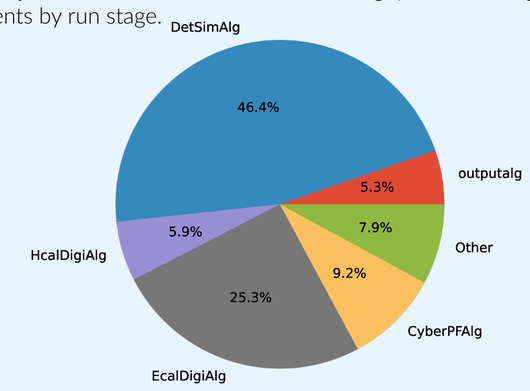

Figure 4. Breakdown of CPU Time Consumption in CEPC Full Simulation

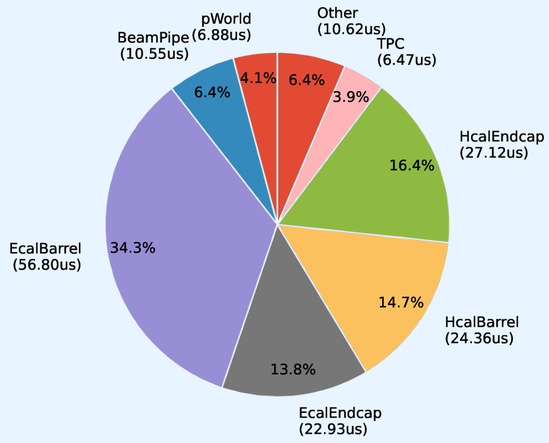

Figure 5. CEPC Geant4 Subdetector Time Profile for $e^+e^- \to q\bar{q}$ at 240 GeV

Fast Simulation and Digitization Flow

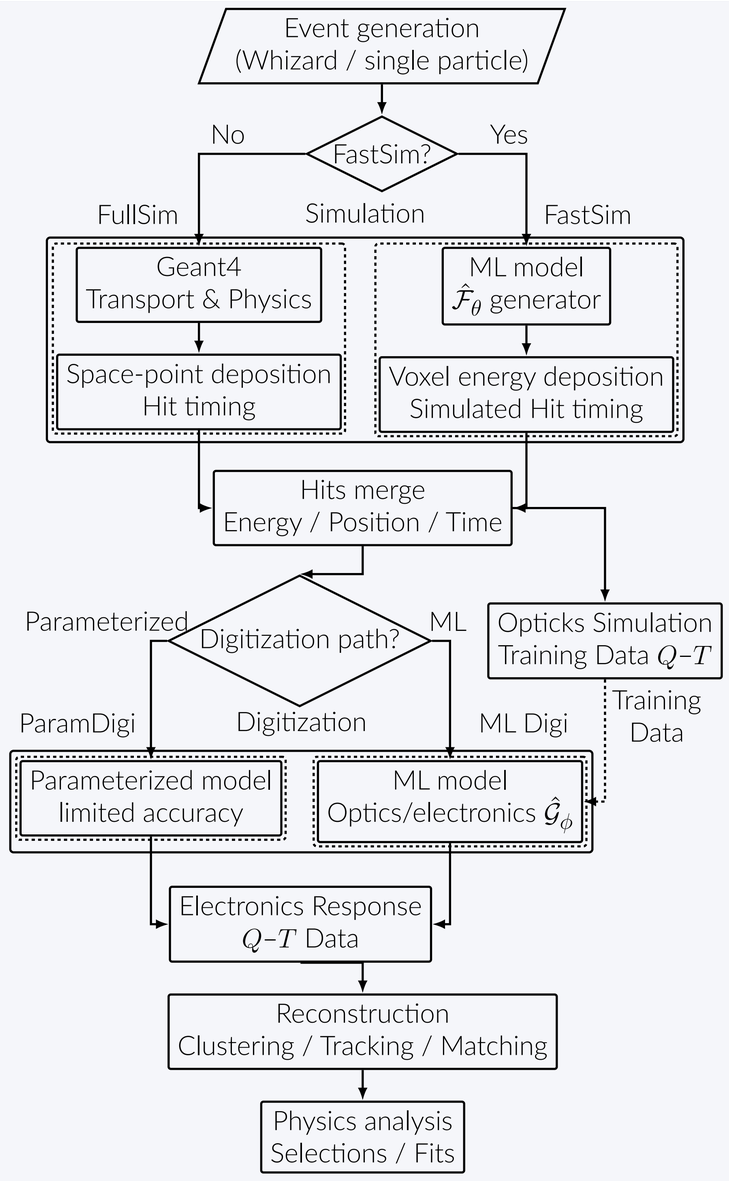

Figure 6. Workflow of CEPC Fast Simulation and Digitization.

Methodology

Fast Simulation

- **Geant4 Data (Baseline):** Collect hits from full `DD4hep` [6] geometry and Geant4 physics, including ID, position, energy, and time.
- **Voxelization:** Convert hits into a $15 \times 15 \times 18$ energy grid and map between global and local coordinates.
- **Dataset:** Combine voxel energies and conditions with normalized phase-space coverage.
- **Model:** Generate $p(V|c)$ under inductive priors (non-negativity, energy conservation, symmetry); export via ONNX [5].
- **Evaluation:** Validate consistency (energy spectra, profiles, EMD, closure) and usability via end-to-end reconstruction.

Figure 7. Fast-simulation data preparation pipeline from Geant4 hits to evaluation metrics.

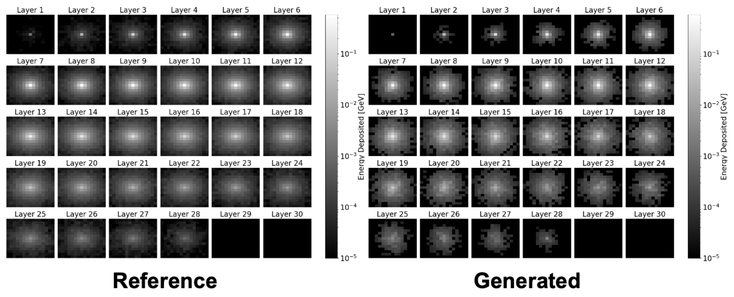

Figure 8. Generative-model shower samples contrasted with reference voxelized energy deposits.

Opticks-Driven Digitization

- **Opticks Data (High-fidelity optical model):** Use `Opticks` [3] + `ElecSim` for per-crystal optical and electronics simulation, generating dual-end readouts $(Q_1, T_1; Q_2, T_2)$ as reference.
- **Feature engineering:** Derive spatio-temporal, geometric, and electronics features (e.g. crystal length, refractive index, noise RMS) with symmetry and normalization preprocessing.
- **Dataset:** Pair features X with optical outputs $R = (Q_1, T_1; Q_2, T_2)$; apply stratified sampling over energy, geometry, and noise conditions.
- **Model:** Train supervised model $\hat{\mathcal{G}}_\phi$ to approximate $\mathcal{G}_{\text{Opticks+elec}}$ using lightweight Transformer or conditional flow networks.
- **Evaluation:** Benchmark against full simulation; check Q, T resolution, $T_1 - T_2$ vs. position linearity, energy resolution, and robustness to noise or drift.

Figure 9. Opticks-driven digitization pipeline from optical truth to evaluation metrics.

Research Objectives

- **Fast ECAL simulation:** Develop ML-based fast simulation reproducing ECAL shower response and morphology with $\mathbf{10–100\times}$ speedup.
- **ML digitization based on Opticks data** Build fast digitization model based on Opticks-generated data which predicting $(Q_{1,2}, T_{1,2})$ with $< 5\%$ residuals and $> 20\times$ acceleration.
- **CEPCSW integration:** Integrate models into CEPCSW via ONNX Runtime for seamless fast/full mode switching.[5]
- **Quantum ML exploration:** Study quantum ML prototypes for improved sample efficiency and lower latency.

Research Progress

Completed investigations

- **Reversible voxelization:** Implemented the bidirectional mapping between DD4hep cellIDs and local (l_x, l_y, l_z) grids with $\delta_\phi = \delta_z = 15$ mm and parity-aware $\delta_r \in \{15, 15.6\}$ mm. The logic swaps axes per `slayer`, wraps modules/staves, clones GAP hits, and enforces energy-sum conservation so ML tensors remain losslessly reversible to native hits.
- **Curriculum photon dataset:** Built the γ dataset (module 0, $\theta = \phi = 90^\circ$) that mirrors the ECAL incident composition/time correlations: $E_k = 256 \cdot 2^{k/2}$ MeV spans 256 MeV–131 GeV with curriculum counts $N(E) = 10^4$ (low-E) down to 10^3 at the tail, totaling $\sim 1.21 \times 10^5$ samples and packaging inputs $(x_0, y_0, z_0, E_{\text{inc}}, \theta, \phi)$ with voxelized outputs.
- **Conditional WGAN-GP baselines:** Deployed the gradient-penalized Wasserstein GAN as the first $p(V \mid c)$ generator.

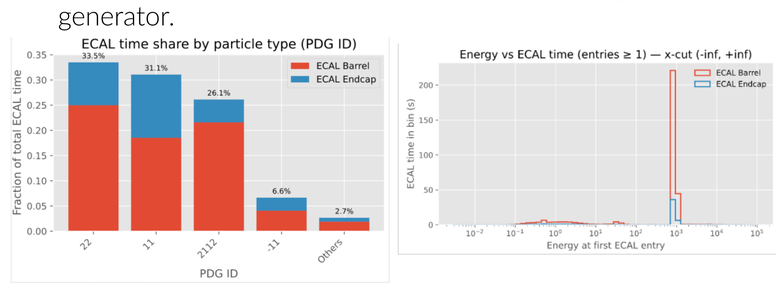

Figure 10. FastSim timing diagnostics: ECAL hit time versus PDGID (left) and incident energy versus ECAL time (right).

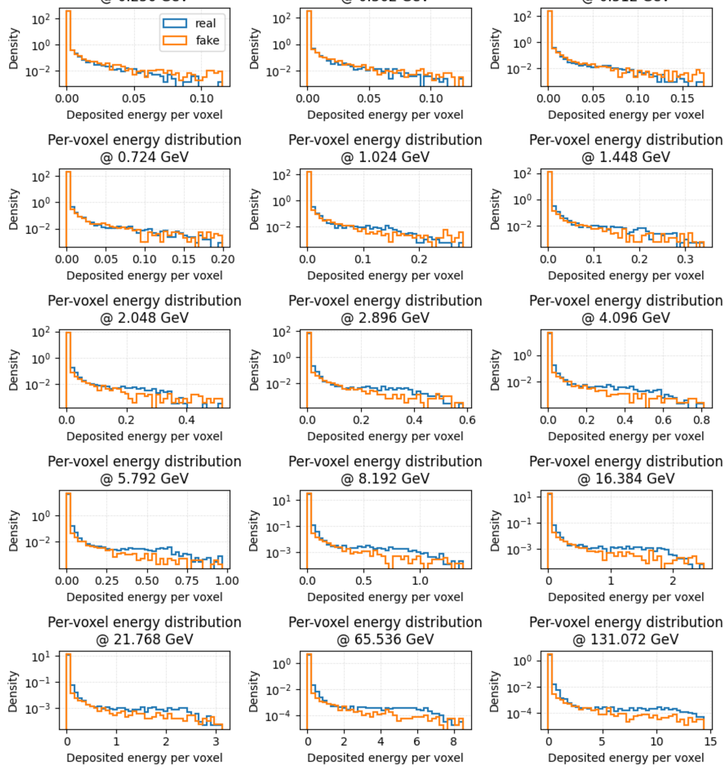

Figure 11. Voxel-level energy spectra from FastSim showers versus Geant4 ground truth for the γ dataset.

Ongoing developments

- **Unified conditioning & capacity control:** Current GAN models can already align the relative voxel-wise energy distributions, but are still under active optimization to reproduce absolute energy distributions and maintain total-energy consistency. We are preparing CNN and flow-based models with stronger energy constraints.
- **Opticks-driven digitization:** Opticks GPU photon transport supplies dual-end Q–T ground truth, and turn it into an FastDigi ML model.[2, 4]
- **CEPCSW integration:** The FastSim/FastDigi pairs are being wrapped in ONNX Runtime execution providers so mixed fast/full pipelines can be profiled inside CEPCSW, targeting $10\times$ ECAL speedup while keeping Higgs recoil mass shifts below 0.1%.
- **Quantum-ML prototypes:** QGAN/QVAE kernels are under study on small photon patches to check if hybrid quantum-classical discriminators can cut the sample count needed for rare angles without compromising latency.

References

[1] Souvik Priyam Adhya et al. "CEPC Technical Design Report - Reference Detector". In: (Oct. 2025). arXiv: 2510.05260 [hep-ex].

[2] Simon C. Blyth. "Opticks: GPU Optical Photon Simulation for Particle Physics using NVIDIA® OptiX™". In: *Proceedings of the International Conference on Computing in High Energy and Nuclear Physics (CHEP 2018)*. Vol. 214. Open Access, CC BY 4.0. EDP Sciences, 2019, p. 02027. doi: 10.1051/epjconf/201921402027.

[3] Simon C. Blyth. *Opticks*. https://bitbucket.org/simoncblyth/opticks/src/master/. Accessed: 2025-09-16.

[4] Simon C. Blyth and JUNO Collaboration. "Meeting the challenge of JUNO simulation with Opticks: GPU optical photon acceleration via NVIDIA® OptiX™". In: *EPJ Web of Conferences*. Vol. 245. Open Access, CHEP 2020. EDP Sciences, 2020, p. 11003. doi: 10.1051/epjconf/202124511003.

[5] ONNX Runtime developers. *ONNX Runtime*. https://onnxruntime.ai/. Version: x.y.z. 2021.

[6] Markus Frank et al. *AIDASoft/DD4hep*. webpage: http://dd4hep.cern.ch/. Oct. 2018. doi: 10.5281/zenodo.592244. url: https://doi.org/10.5281/zenodo.592244.

A Concurrent and Distributed Analysis Framework for Large-Scale High-Energy Physics Experiments

D11

Shuzhu Jin[1], Weidong Li[1], Xiaomei Zhang[1], Tao Lin[1], Jiaheng Zou[1]
[1]Institute of High Energy Physics

Motivation

The upcoming high-energy physics experiments, such as the future CEPC, will generate data at an unprecedented scale, from petabytes to exabytes. This poses a common computational grand challenge: how to process massive datasets efficiently across heterogeneous computing resources. Traditional data processing paradigms often struggle with severe resource under-utilization and performance bottlenecks, particularly due to inefficient I/O operations (e.g., high-latency disk access and network congestion) when handling large-scale datasets. Additionally, these paradigms lack the flexibility to integrate modern machine learning (ML) methods, such as distributed training and real-time inference, which are critical for optimizing complex analysis workflows in hybrid CPU/GPU environments. There is a need for a generic, scalable, and intelligent analysis framework that can dynamically orchestrate tasks and balance loads to fully exploit the potential of modern computing clusters. The concurrent and distributed framework presented here is designed to meet this exact need, holding high applicability for the computational demands of the CEPC project.

Framework Requirements

Accelerate and simplify data analysis process across distributed nodes.

- High-Performance Search: Enable rapid event skimming and filtering in large-scale datasets to identify critical physics signatures efficiently.
- Task Parallelization: Split selection task across multiple nodes
- Self-Balancing Resource Allocation: Intelligent task reassignment to eliminate idle resources.
- Modular design: Integrate traditional analysis algorithms or ML methods in event analysis.

Design Overview

The proposed framework is built on MPI (Message Passing Interface) to enable high-performance, distributed computing for large-scale data processing.

Dynamic Task Scheduler (MPI Scheduler)

- The entire framework relies on MPI for communication, ensuring low-latency, high-throughput task orchestration.
- Implements dynamic task allocation based on workload priorities and resource availability.

CPU Workers: Execute general-purpose computing tasks (e.g., data preprocessing, traditional analysis).

GPU Workers: Work as a service. Accelerate ML workloads (e.g., distributed training, real-time inference) and computationally intensive tasks (e.g., event reconstruction).

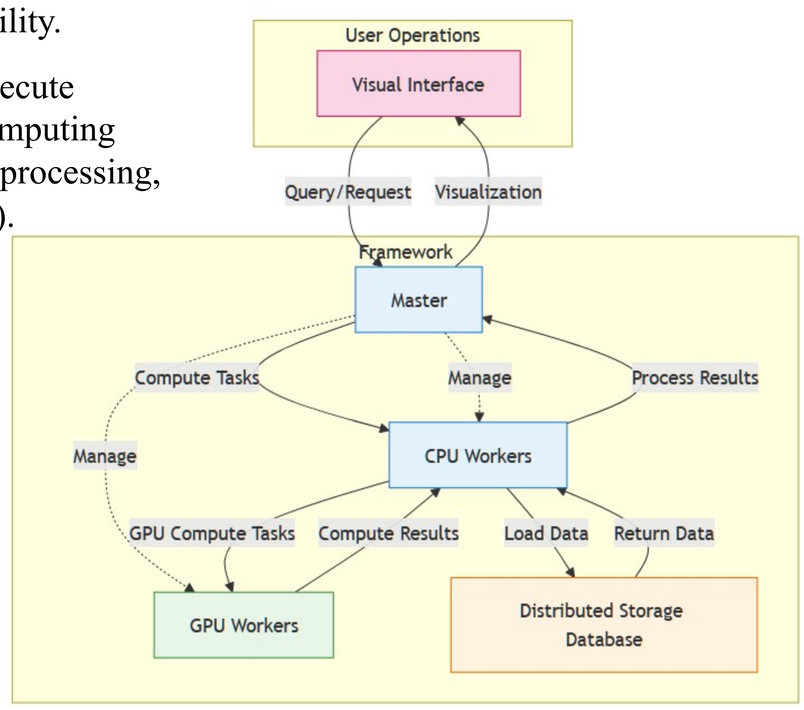

Fig 1. Workflow of the framework

MPI-based Distributed Scheduler

Main thread of MPI-Master:

- Initialization: Open TCP port → Wait for workers → Create worker threads for each worker
- Maintains the connection between the master and workers based on the backend heartbeat mechanism.

Main thread launches two components:

- Worker Threads: Multiple threads (1→n) run in parallel to execute core tasks (e.g., Send different commands to external workers).
- Feedback Thread: Lives within the Feedback System and manages status monitoring/feedback relay.

Feedback system operations:

- The Feedback Thread initiates Monitor Status to track Worker Thread progress or external responses.
- Monitor Status → Check: feedback received? → If Yes, notify the main thread.

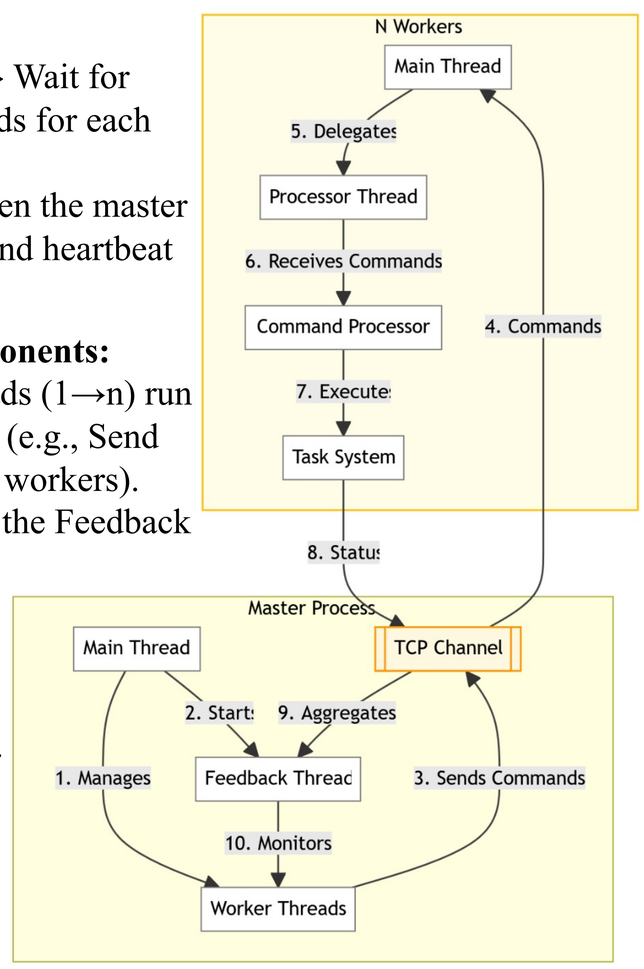

Fig 2. Implement of the scheduler

Implementation of Workers

One Master will manage several Workers. The Worker starts in an idle state, waiting to establish a connection with the Master. After registering with Master, it will receive commands from Master and execute, send status back to Master. The whole process is as below:

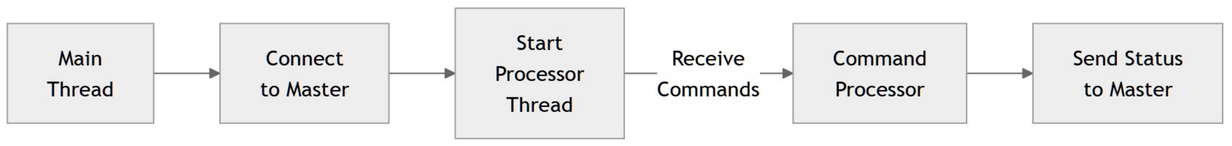

Fig3. Workflow of a worker

Command Processor's Lifecycle

1. Receiving Commands

The Worker continuously listens for commands from the Master, including:

- Task Assignment: Receives specific task descriptions (e.g., which files to process, which algorithms to execute). Worker adds file paths into File Buffer, waits for task execution.
- Control Commands: Such as START, PAUSE, or STOP.

2. Task Execution
Loads required resources (e.g., input files, algorithm configurations) based on the commands. Read files from File Buffer. Regularly updates the Master on task progress, and adjusts task priority or resource allocation based on Master instructions.

3. Termination & Cleanup
After task completion, releases resources and returns to the Idle state, ready for new tasks. If instructed by the Master or finishing all tasks, fully terminates Worker process.

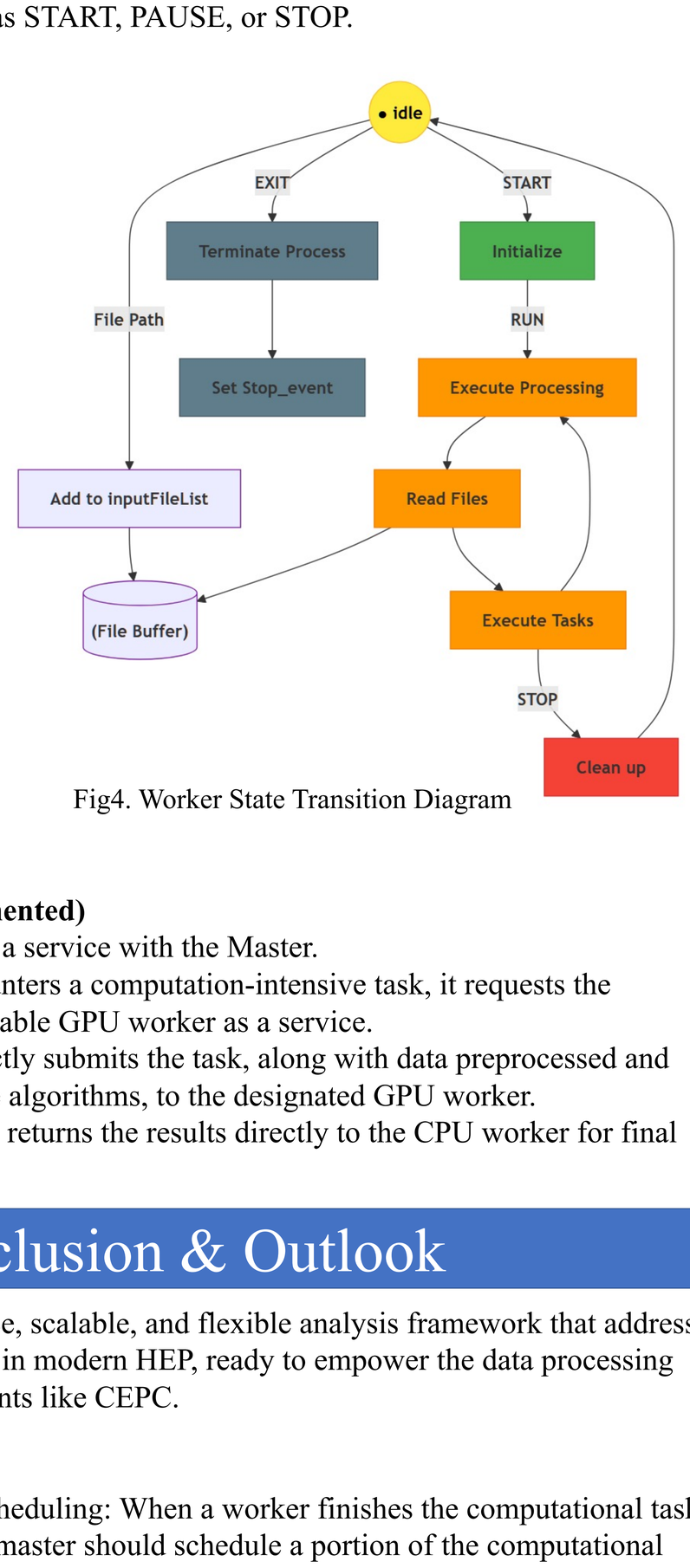

Fig4. Worker State Transition Diagram

GPU Worker (Being implemented)

- GPU nodes first register as a service with the Master.
- When a CPU worker encounters a computation-intensive task, it requests the Master to schedule an available GPU worker as a service.
- The CPU worker then directly submits the task, along with data preprocessed and compressed using real-time algorithms, to the designated GPU worker.
- Upon completion, the GPU returns the results directly to the CPU worker for final integration.

Conclusion & Outlook

We present a high-performance, scalable, and flexible analysis framework that addresses key computational challenges in modern HEP, ready to empower the data processing workflows of future experiments like CEPC.

Future Work:

- Extend to GPU nodes;
- Dynamic task allocation/scheduling: When a worker finishes the computational task first and becomes idle, the master should schedule a portion of the computational tasks from other workers to it.
- Customize and optimize for CEPC's specific computing model.